

Scuola di Scienze
Corso di Laurea Magistrale in Fisica del Sistema Terra

Organic matter deposition/resuspension
in a one-dimensional
physical-biogeochemical model
A modelling study

Relatore:
Prof. Marco Zavatarelli

Presentata da:
Giovanni Ricci

Sessione I
Anno Accademico 2015/2016

Contents

1	Aim of the work and objectives	3
2	The Benthic Boundary Layer	5
2.1	Introduction	5
2.2	Boundary Layer	6
2.3	Benthic Boundary Layer	8
2.3.1	Turbulent Layer	9
2.3.2	Logarithmic Layer	10
2.3.3	”Free stream” Layer	10
3	The deposition/resuspension processes	13
3.1	Introduction	13
3.2	Deposition	14
3.3	Resuspension	14
4	The Model	17
4.1	POM: Princeton Ocean Model	18
4.1.1	Grid arrangement	18
4.1.2	Equations	18
4.2	BFM: Biogeochemical Flux Model	21
4.2.1	Equations	22
4.2.2	Pelagic model	23
4.2.3	Benthic model	26
4.3	The transport model	31
4.4	The sediment deposition/resuspension model	32
4.4.1	Particulate organic matter flux calculation at the sediment- water interface	32
4.4.2	Stresses calculation	35
4.5	Coupling	38

4.5.1	Source Splitting	40
5	Implementation	41
5.1	Adriatic Sea	41
5.2	Data inputs	44
5.3	Waves	46
5.4	Bottom stress	47
5.5	Experiments definition	48
6	Results	51
6.1	ORIGINAL case: no resuspension	51
6.2	BASE case: mean current resuspension	53
6.3	BaseW case: base-wave resuspension	56
6.4	Peak I: W1-W2-W3 cases	58
6.5	Peak II: W4-W5-W6 cases	62
6.6	Peak III: W7-W8-W9 cases	65
7	Discussion	69
7.1	Maximum bottom stress calculation	69
7.2	Resuspension and mixing conditions	71
7.3	Phytoplankton/bacteria relationship during the resuspension event .	74
8	Conclusions	77

Abstract

The shallow water configuration of the gulf of Trieste allows the propagation of the stress due to wind and waves along the whole water column down to the bottom. When the stress overcomes a particular threshold it produces resuspension processes of the benthic detritus. The benthic sediments in the North Adriatic are rich of organic matter, transported here by many rivers. This biological active particulate, when remaining in the water, can be transported in all the Adriatic basin by the basin-wide circulation.

In this work is presented a first implementation of a resuspension/deposition sub-model in the oceanographic coupled physical-biogeochemical 1-dimensional numerical model POM-BFM.

At first has been considered the only climatological wind stress forcing, next has been introduced, on the surface, an annual cycle of wave motion and finally have been imposed some exceptional wave event in different periods of the year.

The results show a strong relationship between the efficiency of the resuspension process and the stratification of the water column. During summer the strong stratification can contained a great quantity of suspended matter near to the bottom, while during winter even a low concentration of particulate can reach the surface and remains into the water for several months without settling and influencing the biogeochemical system.

Looking at the biologic effects, the organic particulate, injected in the water column, allow a sudden growth of the pelagic bacteria which competes with the phytoplankton for nutrients strongly inhibiting its growth. This happen especially during summer when the suspended benthic detritus concentration is greater.

Chapter 1

Aim of the work and objectives

In a shallow water system, the processes of interaction of the water column with the benthic domain are very important, since the biogeochemical processes occurring between the pelagic and the benthic domain are very tight.

The purpose of this work is to provide an initial evaluation of the importance of the deposition/resuspension processes through a newly implemented parametrization of such processes in a numerical physical-biogeochemical model of the coastal marine ecosystem. The implementation accounts for the surface waves role in determining the bottom stress conditions modulating both the sediments sinking and resuspension.

The model is composed by the Princeton ocean model, POM (Blumberg and Mellor (1987)) and the Biogeochemical Flux Model, BFM (Vichi et al. (2015)). The modified sediment deposition / resuspension model developed by Wang and Pinardi (2002) has been inserted into such system and applied to the benthic-pelagic coupling processes involving the particulate organic matter, with the aim to explore the impact of the deposition / resuspension process on the biogeochemical dynamics.

Chapter 2

The Benthic Boundary Layer

2.1 Introduction

The variability of the ocean vertical structure is mainly determined by the prevailing forcing conditions.

The governing equation system, for the ocean fluid dynamics, under the hydrostatic and Boussinesq approximations, is given by:

the momentum equation:

$$\frac{\partial \vec{u}}{\partial t} + \underbrace{(\vec{u} \cdot \vec{\nabla}) \vec{u}}_{\text{advection}} + \underbrace{\vec{f} \times \vec{u}}_{\text{Coriolis}} = \frac{1}{\rho} \vec{\nabla} p + \vec{g} + \underbrace{\frac{(K_h + \mu)}{\rho} \nabla_h^2 \vec{u} + \frac{(K_v + \mu)}{\rho} \frac{\partial^2 \vec{u}}{\partial z^2}}_{\text{Viscous forces}} \quad (2.1)$$

the continuity equation:

$$\frac{\partial \rho}{\partial t} + \vec{u} \cdot \vec{\nabla} \rho = -\rho \vec{\nabla} \cdot \vec{u} \quad (2.2)$$

the hydrostatic equation, assuming constant density: $\rho = \rho_0$

$$\frac{\partial p}{\partial z} = -\rho g \quad (2.3)$$

where:

$\vec{u} = (u, v, w)$ is the velocity tridimensional vector;

$p = p(z)$ is the pressure;

$\rho = (T, S, p)$ is the density;

$\vec{f} = 2\vec{\Omega} = 2\Omega (\cos\theta\hat{j} + \sin\theta\hat{k})$ is the Coriolis parameter;

$\vec{g} = -g\hat{k}$ is the gravity acceleration ($g = 9.81ms^{-2}$);

$\nabla_h^2 = \frac{\partial^2}{\partial x^2} + \frac{\partial^2}{\partial y^2}$ is the horizontal laplacian vector;

K_h, K_v are the horizontal and vertical turbulent viscosity coefficients (here considered constant in space and time);

μ is the viscous molecular coefficient.

The viscous forcing is considered negligible in the interior of the sea, but at the ocean surface and bottom boundary layers it becomes important and generates the so-called boundary layers.

2.2 Boundary Layer

A Boundary Layer (hereafter called BL) in fluid dynamics is the part of fluid immediately close to a bounding surface that divides two fluids or a fluid and a solid surface with different physical properties (velocity, density ...). In this zone the viscous effects are significant.

Viscosity can be introduced considering a mass of water inserted between two planes, one fixed (bottom side) and one moving at a constant velocity \vec{U} parallel to the surface of the planes. The water near the moving plane starts to move until is reached a steady vertical profile of water velocity $u(z)$.

Now is considered a laminar BL thus it's not characterized by turbulent motions (K_v is negligible). In this case the velocity profile is linear (Figure 2.1).

To balance the force applied by the plane on the fluid is necessary the presence of the shear stress (τ) proportional to the velocity profile:

2.2 Boundary Layer

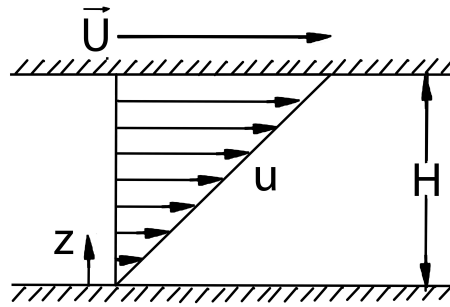


Figure 2.1: Laminar regime for a fluid between two planes, the one on the top moving with velocity \vec{U} .

$$\tau = \mu \frac{\partial u}{\partial z} \quad [N/m^2 \equiv Pa]$$

This is the so-called Newton viscosity law.

μ is the constant of molecular viscosity, that depends on the physical-chemical properties of the fluid. The force for unit of mass generated by the shear stress can be computed as:

$$\frac{F}{m} = \frac{1}{\rho} \frac{\partial \tau}{\partial z} = \frac{\mu}{\rho} \frac{\partial^2 u}{\partial^2 z} = \nu \frac{\partial^2 u}{\partial^2 z}$$

The quantification of the dominance of the viscous effects on the turbulent effects is done through the Reynolds number. It's defined as :

$$Re = \frac{\text{inertial forces}}{\text{viscous forces}} = \frac{U l}{\nu}$$

where U is the magnitude of the velocity, l is the space length scale.

The two different regimes could be identified according to the Re value:

- Laminar \rightarrow low values of Re : the viscous forces prevail and the flow is characterized by smooth and constant fluid motion.
- Turbulent \rightarrow high values of Re : the inertial forces prevail and the flow becomes turbulent with chaotic eddies and vortexes.

There is not a unique threshold between the two states, but it varies for every situation. For the planetary scale the Reynolds number is of the order of 10^6 and the turbulent regime is always verified.

This is right in the case of the Benthic Boundary Layer (BBL) which is the subject of this study. The behavior of the lowest part of the ocean is directly influenced by its contact with the bottom (seabed), here dominated by turbulent dynamics.

2.3 Benthic Boundary Layer

The BBL has a complex structure and is characterized by different dynamical conditions depending also on the distance from the seabed.

The 3 different regions that can be identified (Figure 2.2) are:

- Viscous
- Logarithmic
- Turbulent

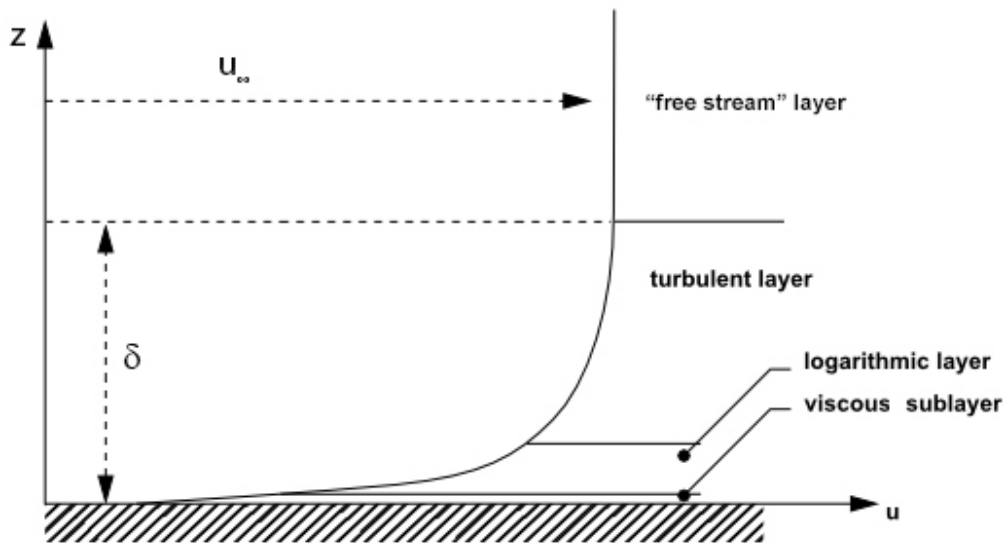


Figure 2.2: Profile of the BBL. δ is the thickness of the BBL and u_∞ the module of the geostrophic velocity.

Above the turbulent layer there is the "free stream" layer where the bottom influence is negligible.

Viscous Layer

This layer is dominated by viscous forces. The shear stress τ_b varies slowly with the height and could be considered constant.

2.3 Benthic Boundary Layer

The features of the flow in the viscous layer strictly depend on the bottom surface characteristics which are determined by the value of Reynolds number (referred to the roughness's conditions) computed as follow:

$$R_{er} = \frac{u_{*B}^2 d}{K_v}$$

where d represents the characteristics dimension of the roughness elements.

In a turbulent regime the molecular viscosity (μ) is considered negligible compared to the turbulent vertical viscosity (K_v) which regulates the proportionality between the shear stress and the mean velocity profile.

u_* the friction velocity is defined as

$$u_* = \sqrt{\frac{\tau}{\rho}}$$

Three different regimes can be identified according to R_{er} :

1. Smooth viscous turbulent $R_{er} < 5.5$
2. Transient $5.5 < R_{er} < 165$
3. Rough viscous turbulent $R_{er} > 165$

The first one is quite a laminar flow while the last one is characterized by the formation of eddies and vortices because of the roughness elements determining the benthic surface which are exceeding the thickness of the viscous layer. An example of rough surface is a seabed formed by sand waves and rocks.

2.3.1 Turbulent Layer

The viscous layer is very thin, so quite all the BL manifests a turbulent regime.

The turbulent shear stress, for a zonal velocity field ($\vec{u} = |\vec{u}| \hat{i}$), is:

$$\tau_{xz} = -\rho \overline{u'w'}$$

where (u', v', w') are the three components of the turbulent velocity field (fluctuations). To solve this equation is used the empirical turbulent closure with which is possible to define the turbulent shear stresses as a function of the mean velocity field:

$$\tau_{xz} = \rho_0 K_v \frac{\partial \bar{u}}{\partial z}$$

K_v is the vertical turbulent viscosity coefficient. This is large in the BL and fall down fast out of it.

2.3.2 Logarithmic Layer

The Logarithmic Layer is the layer above the bottom surface high enough to be influenced by the geometry of the surface, but not high enough to be exclusively influenced by the "free stream". The shear stresses have at the lower and upper boundaries of this layer, respectively, viscous and turbulent conditions at which they have to tend.

This layer is so called because of the vertical profile of the velocities, which is defined by a Wall Law:

$$\vec{u}(z) = \frac{u_{*B}^2}{\kappa} \log\left(\frac{z}{z_0}\right) \quad (2.4)$$

where z_0 is the physical roughness length, κ is the constant of Von Karman (0.4 is a good approximation). The presence of κ derived from the experimental approximation of the turbulent viscosity K_v which, in this layer, grows with the distance from the benthic: $K_v = \kappa z$.

This profile is proportional to the bottom stress through the drag coefficient C_d :

$$\tau_b = \rho C_d |\vec{u}(z_r)|^2 \quad (2.5)$$

where z_r is the reference height for the viscous layer.

The drag coefficient could be computed as follow:

$$C_d = \left(\frac{\kappa}{\log(z_r/z_0)}\right)^2 \quad (2.6)$$

2.3.3 "Free stream" Layer

Out of the BBL the turbulent components are negligible and the N-S equation can be rewritten:

$$\frac{D\vec{u}}{Dt} + \vec{f} \times \vec{u} = \frac{1}{\rho} \vec{\nabla} p \quad (2.7)$$

2.3 Benthic Boundary Layer

Imposing the steady conditions are obtained the geostrophic equations which rule this layer:

$$fv_g = \frac{1}{\rho} \frac{\partial p}{\partial x}$$

$$fu_g = -\frac{1}{\rho} \frac{\partial p}{\partial y}$$

Where $(u_g, v_g) = u_\infty$ (see Figure 2.2).

It could happen that the thickness of the two BLs (atmosphere-water at top and water-seabed at bottom) overcome the height of the water column. In this case there's not a "free stream" layer.

Chapter 3

The deposition/resuspension processes

3.1 Introduction

The deposition/resuspension processes are important in the coastal shallow environment, where the role of the bottom stress is significant. Once the particulate matter is suspended in the water, if no important horizontal currents arise, it undergoes the gravity force and slowly returned to the seabed with a sinking velocity dependent on the fluid dynamic of the system particle-water.

The vertical motion of the suspended matter is defined by an advective and a diffusive components, and at every layer is valid:

$$\frac{\partial C}{\partial t} = - (w + w_s) \frac{\partial C}{\partial z} + \frac{\partial}{\partial z} \left(K_v \frac{\partial C}{\partial z} \right)$$

where C is the concentration of the particulate, w and w_s are the water and sediments vertical velocity respectively.

Sediment flux at the bottom (integrated on the last layer) is the difference between the deposition rate (D) and erosion rate (R), so that

$$- (w + w_s) C + K_v \frac{\partial C}{\partial z} = D - R$$

The bottom resuspension rate (R) is zero if the bottom shear stress (τ_b) is below a critical value (τ_{crit}). The resuspended matter modifies the bottom concentrations and so the diffusive motion (depending on the vertical gradient of C).

Many studies have been carried out about the sediment resuspension and transport processes. Here the theory adopted is based mostly on McDonnell and Buesseler (2010) and Southard (2006) built on the work of Shields A. (1936).

3.2 Deposition

The deposition process has been widely studied because of its complexity (McDonnell and Buesseler (2010); Clarke and Elliot (1998)). Indeed the suspended particulate shows a large variability in size and shape determining broad changes in the characteristic of the interaction with the fluid.

This work has not the aim of describe in depth this process, thus, for simplicity, hereafter the particles are considered spherical and of a specific radius.

Particle deposition flux can be described as the product of the particle concentration and the sinking velocity. Different studies have provided a wide range of measured sinking rates, due to measurement uncertainty, but also to real variability in sinking rates at different times and places due to complex factors such as fluid viscosity, particle source material, morphology, porosity, density, and other variable particle characteristics. Even though no simple relationships have been discovered, a good representation of the sinking velocity w_s is defined by the Stokes' law (spherical particle):

$$w_s = \frac{gd^2}{18\nu} \left(\frac{\rho_s}{\rho_w} - 1 \right) \quad (3.1)$$

where d is the radius of the particle, g the gravity acceleration, ν the kinetic viscosity and ρ_s and ρ_w are the sediments and water densities. In the modelling work at the base of this thesis Equation 3.1 has been adopted to compute w_s .

3.3 Resuspension

The resuspension process is described considering by a representative sediment particle resting on the surface of a cohesionless sediment bed at the water-sediment interface of a flowing fluid. If the fluid is not moving fast enough to move the particle, then the particle is motionless. The forces applied to particles are of three kinds: particle weight, fluid forces and particle-to-particle contact forces.

3.3 Resuspension

The contact forces are considered negligible here.

The resultant of the weight and the fluid forces determines the state of the particles (quiet or motion). The weight force is easily defined as the difference between the weight and the buoyancy as: $\gamma = (\rho_s - \rho_w) g$.

The fluid forces are more difficult to be defined. These are generated by the water flow on the sediments (tangential to the surface) and their resultant could change in direction and module according to the characteristics of the flow. The main parameter, determining this force, is the Reynolds number already introduced in chapter 2. For high values of Re the turbulent regime is established and, at the interface, vortexes are generated which generate a forcing normal to the surface and opposed to the gravity force (Figure 3.1).

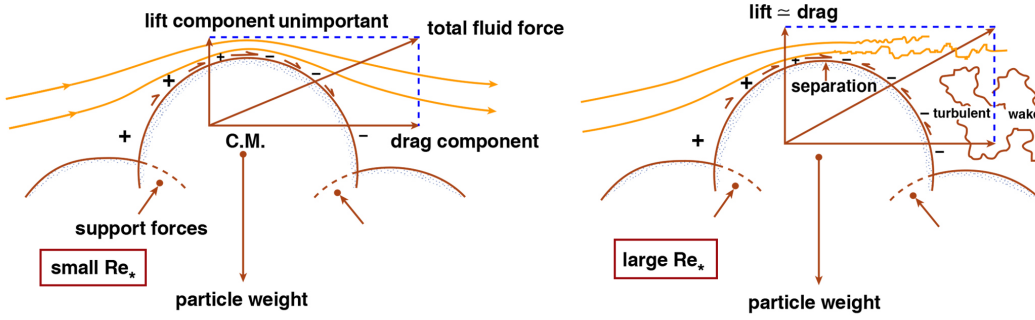


Figure 3.1: Different features of the sediments equilibrium with different Re values. Figure by Southard (2006).

This forcing is proportional to the bottom shear stress already defined. When the stress overcomes a critical value, the fluid forcing overcome the gravity forcing and resuspension start.

This basic criterion for the initiation of motion can be written as: $\tau_b \geq \tau_{crit}$ where τ_b is the bottom shear stress and τ_{crit} the threshold value.

This is typically represented by a comparison between a dimensionless shear stress (τ_b^*) and a dimensionless critical shear stress (τ_{crit}^*), in order to compare the two different kind of force. The dimensionless shear stress τ_b^* is called Shields parameter and is defined as:

$$\tau_b^* = \frac{\tau_b}{(\rho_s - \rho_w)gd} \quad (3.2)$$

The new equation to solve becomes: $\tau_b^* \geq \tau_{crit}^*$.

Only one size of particle is considered in this equation. This is a good approximation for the seabed, but not for a river discharge region which contains sediments with a lot of different shapes and dimension.

The τ_{crit}^* factor depends on the hydraulic conditions near the bed, the particle shape and the particle position relative to the other particles. The hydraulic conditions near the bed can be expressed by the Reynolds number $Re^* = u^*d/\nu$ (u^* is the friction velocity and ν is the kinematic viscosity).

Thus the Shields parameter (τ_{crit}^*), should be expected to be a function of grain geometry and boundary Reynolds number:

$$\tau_{crit}^* = f(Re^*)$$

Many experiments have been performed to determine the τ_{crit}^* value as a function of Re^* . The experimental results of Shields (1936) related to a flat bed surface are most widely used to represent the critical conditions for initiation of motion.

This allows us to rewrite the criterion for the initiation of motion in terms of only needing to solve for a specific version of the Reynolds number:

$$\tau_b^* = \frac{\tau_b}{(\rho_s - \rho_w)gd} \geq f(Re^*)$$

This equation can then be solved by using the empirically derived Shields curve to find τ_{crit}^* . Different mathematical solutions have been generated.

Determined the activation of the resuspension process the flux of matter (R) is defined as the deposition one: velocity of resuspension (w_{res}) times the sediments concentration (C_s). This basic flux has to be modulated by the value of the shear stress, in fact it's directly proportional to τ_b (Chao (1998)):

$$R = w_{res}C_s \left(\frac{\tau_b}{\tau_{crit}} - 1 \right)$$

Chapter 4

The Model

The physical processes are fundamental for the biogeochemical dynamics of marine environment since determine availability of resources and location and transport of biomass.

Very important is also the evaluation of the different field variables, such as temperature and oxygen concentration, since they modulate biological processes such as growth, respiration and mortality.

The phytoplankton spring bloom is an example of the influence of physics in the biogeochemical processes. It heavily depends on particular physical state variables (radiation, temperature profile, salinity ...) and, when the conditions are verified, it triggers the important growth of the phytoplankton on the upper layers. A good approach to face such a complex system is to divide it in two separate sub-models each of them separately applicable to:

- an Eulerian ocean circulation model: treats the physical variables of the environment and provides them to the biogeochemical model;
- an ecological system: describes biologically the biota and its biogeochemical fluxes.

Another component has to be added to these two blocks: the Transport model that handles the advective and diffusive transport of the biogeochemical state variables. The one-dimensional coupled numerical model used is composed of the one-dimensional version of the Princeton Ocean Model (POM) (Blumberg and Mellor (1987)) and the Biogeochemical Flux Model (BFM) (Vichi et al. (2007)).

This section briefly explains the structure of the different models and the coupling scheme.

4.1 POM: Princeton Ocean Model

The Princeton Ocean Model (POM) (Blumberg and Mellor (1987)) is a free surface, finite difference, sigma coordinate general circulation model.

The 3D model prognostically calculates surface elevation, velocities, temperature, salinity and vertical diffusion coefficients. However in this revised 1D model the climatological time dependent (monthly varying) temperature and salinity vertical profiles are obtained from data and imposed to the system (see chapter 5).

This diagnostic approach eliminates possible drifts in temperature and/or salinity due to the use of a "non zero" surface heat and/or mass surface fluxes. This overcomes the lack of a proper parametrization of the lateral advective fluxes, which are, by necessity, not contained in a one-dimensional model implementation.

The vertical profiles of vertical diffusion coefficients are computed by the model through a second order turbulence closure proposed by Mellor and Yamada (1982).

4.1.1 Grid arrangement

The velocities and concentration variables are placed in scattered vertical grids.

The vertical variable σ is defined as:

$$\sigma = \frac{z}{H}$$

where H is the bottom depth. σ varies from -1 (at $z = -H$) to 0 (at $z = 0$).

Layers are linearly distributed in the water column interior and logarithmically distributed near the bottom and surface: such a discretization is done for having a better definition of the two BL.

4.1.2 Equations

The model is based on the Navier-Stokes equations for geophysical flow in a rotating coordinate system. The pressure, as written previously, is assumed to be in hydrostatic equilibrium and density differences are considered only in gravitational forces (Boussinesq approximation).

$$\begin{aligned} \frac{\partial u}{\partial t} - fv &= \frac{\partial}{\partial z} \left(K_m \frac{\partial u}{\partial z} \right) \\ \frac{\partial v}{\partial t} + fu &= \frac{\partial}{\partial z} \left(K_m \frac{\partial v}{\partial z} \right) \\ \frac{\partial p}{\partial z} &= -\rho g \end{aligned}$$

4.1 POM: Princeton Ocean Model

where (u, v) are the velocities of the mean circulation and K_m is the turbulent diffusivity defines as $K_m = qlS_m$, where l is the turbulent length scale; q is the turbulent kinetic energy; S_m is an empirical function (Mellor and Yamada (1982)).

The variation of the turbulent kinetic energy $q^2/2$ is calculated with:

$$\frac{\partial}{\partial t} \left(\frac{q^2}{2} \right) = \frac{\partial}{\partial z} \left(K_m \frac{1}{2} \frac{\partial q^2}{\partial z} \right) + P_s + P_b - \epsilon$$

P_s is the production for shear; P_b the buoyant dissipation/production ; ϵ the turbulent dispersion.

The dynamic conditions at the boundary consider the forcing of the oceanic circulation at the air-water interface as the heat, water and momentum fluxes. The principal one is the momentum flux which depends on the wind stress. At the BBL the dynamic equilibrium is between the moving water and the seabed.

Boundary conditions

At the surface the wind transmits momentum to the water. The equilibrium equations are defined equaling the wind stress with the ocean shear stress for the two different directions:

$$K_m \frac{\partial u}{\partial z} \Big|_{z=0} = \vec{\tau}_w^x; \quad (4.1a)$$

$$K_m \frac{\partial v}{\partial z} \Big|_{z=0} = \vec{\tau}_w^y \quad (4.1b)$$

where $\vec{\tau}_w$ is an external imposing.

At the benthic boundary layer the dynamic condition is the same defined in chapter 2. Close to the interface is valid the wall law and the equations 2.5 and 2.6:

$$K_m \frac{\partial u}{\partial z} \Big|_{z=-H} = \vec{\tau}_b^x; \quad (4.2a)$$

$$K_m \frac{\partial v}{\partial z} \Big|_{z=-H} = \vec{\tau}_b^y \quad (4.2b)$$

In the model, the drag coefficient, coherently with the theory described in chapter 2, is defined with a lowpass limit value:

$$C_d = Max \left\{ \left[\frac{0.4}{\log \left(\frac{H+z_r}{z_0} \right)} \right]^2, 0.0025 \right\} \quad (4.3)$$

where $z_0 = 0.01m$ is the roughness length and $z_r = zz_{KB-1}$ is the reference depth, the depth of the last layer. Since zz_{KB-1} is a constant in the model, $C_d \cong 0.237$.

The bottom stress is defined:

$$|\vec{\tau}_b| = \rho C_d (u_b^2 + v_b^2) \quad (4.4)$$

where (u_b, v_b) are the two component of the mean current at the bottom layer.

The two stresses $\vec{\tau}_w$ and $\vec{\tau}_b$ are used to defined the friction velocities $\vec{u}_{*w} = \sqrt{\vec{\tau}_w/\rho}$ and $\vec{u}_{*b} = \sqrt{\vec{\tau}_b/\rho}$ which are needed to define the boundary conditions for the turbulent kinetic energy.

For the kinetic turbulent energy q^2 is used a semi-empirical equation:

$$\frac{q^2}{2} \Big|_{z=0} = B_1^{2/3} |\vec{u}_{*w}| \quad (4.5a)$$

$$\frac{q^2}{2} \Big|_{z=-H} = B_1^{2/3} |\vec{u}_{*b}| \quad (4.5b)$$

where $B_1 = 16.6$.

4.2 BFM: Biogeochemical Flux Model

4.2 BFM: Biogeochemical Flux Model

The open source BFM (Vichi et al. (2015); Vichi et al. (2006); <http://bfm-community.eu/>) is a numerical model for the simulation of the dynamics of major biogeochemical properties in marine ecosystem.

Is a biomass and functional group based marine ecosystem model, representing the system in Eulerian coordinates by a selection of chemical and biological processes that simulates the pelagic (water column) dynamics in the marine ecosystem.

The carbon, nitrogen, phosphorus and silicon biogeochemical cycles are solved independently over a variety of Chemical Functional Groups (CFFs) and Living Functional Groups (LFGs) (see Figure 4.1). CFFs incorporate certain biogeochemical elements contained in complex living and non-living components, and are divided into three main groups:

- non-living organic (particulate and dissolved organic detritus)
- living-organic (LO) (bacteria, phytoplankton, zooplankton, benthic fauna)
- inorganic (IO) (nutrient salts, Oxygen, Carbon dioxide)

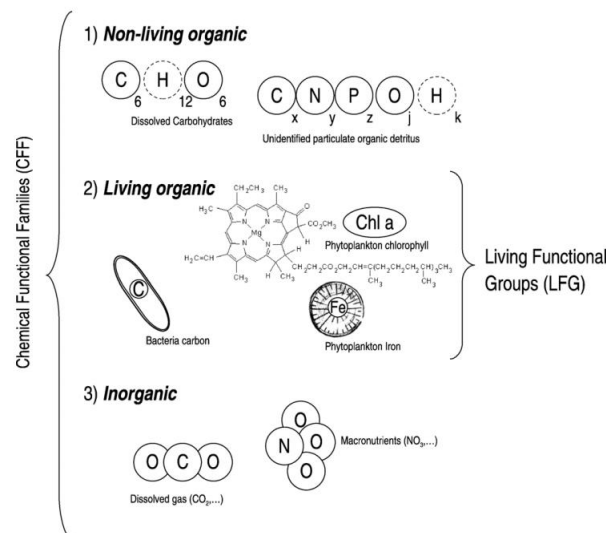


Figure 4.1: The definition of CFFs and LFGs. Image by Butenschön et al. (2012)

These groups are defined by their chemical compositions (Carbon (C); Nitrogen (N); Phosphorus (P); Silicon (S); Oxygen (O) and chlorophyll (chl)).

LFGs represent the whole biota and can be divided into three functional types: producers (phytoplankton), consumers (micro- and meso-zooplankton and benthic

fauna) and decomposers (bacteria). The dynamics of each of these are described by population processes (growth, migration, mortality) and physiological processes (photosynthesis, ingestion, respiration, excretion, egestion).

All the information about the equations used in the model could be found in the Vichi et al. (2015). Here are not reported all the equations, but only a summary .

4.2.1 Equations

Each variable of the BFM is a multidimensional array characterized by one-to-five different constituents (subscript) while the superscript indicates the CFF. For example we consider the Particulate Organic Detritus R^6 :

$$R_i^6 \equiv \{R_c^6, R_n^6, R_p^6, R_s^6\}$$

As defined by its Carbon (R_c^6), Nitrogen (R_n^6), Phosphorus (R_p^6) and Silicon (R_s^6) content. Similarly Phytoplankton, in the diatoms class, is defined as:

$$P_i^1 \equiv \{P_c^1, P_n^1, P_p^1, P_s^1, P_l^1\}$$

where P_l^1 is the chlorophyll content. The rate of change due to biogeochemical processes and relative to each state vector component is given by an equation of the type

$$\left. \frac{\partial C}{\partial t} \right|_{bio} = \left. \frac{\partial C}{\partial t} \right|_{p_1}^{\xi_1} + \dots + \left. \frac{\partial C}{\partial t} \right|_{p_n}^{\xi_n}$$

where subscripts p_i indicate the process (see Table 4.1) and the superscripts ξ_i refer to the state variable playing the counterpart in the process. Mass conservation imposes that: $\left. \frac{\partial c_1}{\partial t} \right|_{p_1}^{\xi_1} = - \left. \frac{\partial \xi_1}{\partial t} \right|_{p_1}^{c_1}$.

4.2 BFM: Biogeochemical Flux Model

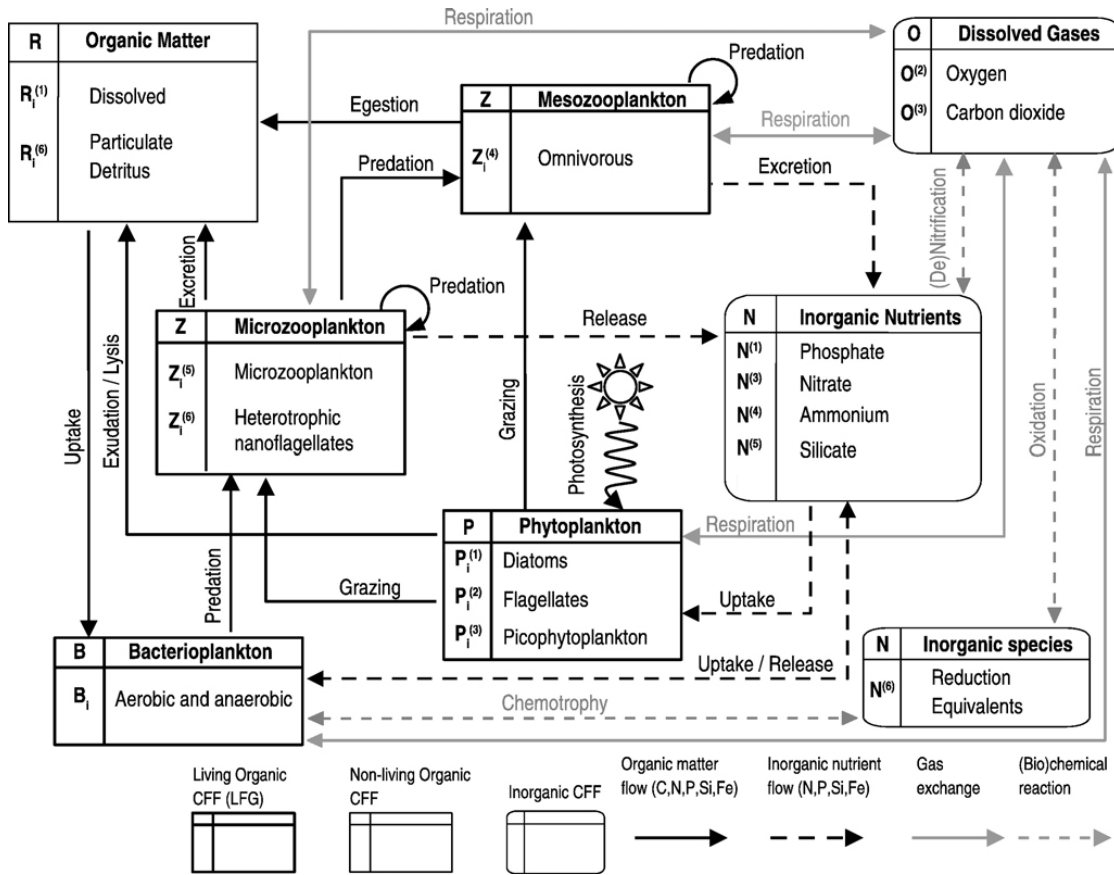


Figure 4.2: BFM pelagic system representation. Image taken by Vichi et al. (2007)

4.2.2 Pelagic model

The three LFG are characterized by the processes shown in Figure 4.2. Below are reported a simplification of the equation for the Phytoplankton (P), the Zooplankton (Z) and Bacteria (B):

$$\begin{aligned}
 \frac{\partial P}{\partial t} \Big|_{bio} &= \frac{\partial P}{\partial t} \Big|_{upt} - \frac{\partial P}{\partial t} \Big|_{exu} - \frac{\partial P}{\partial t} \Big|_{lys} - \frac{\partial P}{\partial t} \Big|_{res} - \frac{\partial P}{\partial t} \Big|_{graz} \\
 \frac{\partial Z}{\partial t} \Big|_{bio} &= \frac{\partial Z}{\partial t} \Big|_{ing} - \frac{\partial Z}{\partial t} \Big|_{ege} - \frac{\partial Z}{\partial t} \Big|_{resp} - \frac{\partial Z}{\partial t} \Big|_{pred} \\
 \frac{\partial B}{\partial t} \Big|_{bio} &= \frac{\partial B}{\partial t} \Big|_{upt} - \frac{\partial B}{\partial t} \Big|_{remin} - \frac{\partial B}{\partial t} \Big|_{res} - \frac{\partial B}{\partial t} \Big|_{pred}
 \end{aligned} \tag{4.6}$$

All the subscripts refer to specific processes (see Table 4.1).

Virtually all processes in the ecosystem depend on the water temperature T . This is modelled by a regulating factor

$$f^T = Q_{10}^{\frac{T-10}{10}} \tag{4.7}$$

Abbreviation	Process
<i>upt</i>	Uptake
<i>exu</i>	Exudation
<i>lys</i>	Lysis
<i>graz</i>	Grazing
<i>ing</i>	Ingestion
<i>resp</i>	Respiration
<i>pred</i>	Predation
<i>remin</i>	Biochemical remineralization

Table 4.1: Abbreviation of some processes in BFM.

where Q_{10} is a parameter specific to each LFG.

Moreover, primary production is heavily depending on light available defined as photosynthetically available radiation (PAR) and distributed along the water column according to the Lambert-Beer formulation

$$I = \frac{Q_s}{\rho c_p} \epsilon_{PAR} \exp \left\{ \int_0^z [\lambda_w(\zeta) + \lambda_{bio}(\zeta)] d\zeta \right\}, \quad (4.8)$$

where Q_s is the solar radiation, ϵ_{PAR} gives the fraction of photosynthetically available radiation, λ_w is the background extinction of water particles and λ_{bio} is the extinction due to phytoplankton, particulate detritus and suspended inorganic matter.

4.2 BFM: Biogeochemical Flux Model

Variable	Code	Type	Const.	Units	Description
$N^{(1)}$	N1p	IO	P	mmol P m ⁻³	Phosphate
$N^{(3)}$	N3n	IO	N	mmol N m ⁻³	Nitrate
$N^{(4)}$	N4n	IO	N	mmol N m ⁻³	Ammonium
$N^{(5)}$	N5s	IO	Si	mmol Si m ⁻³	Silicate
$N^{(6)}$	N6r	IO	R	mmol S m ⁻³	Reduction equivalents, HS ⁻
$N^{(7)}$	N7f	IO	Fe	μ mol Fe m ⁻³	Dissolved Iron
$O^{(2)}$	O2o	IO	O	mmol O ₂ m ⁻³	Dissolved Oxygen
$O^{(3)}$	O3c	IO	C	mg C m ⁻³	Dissolved Inorganic Carbon
$O^{(5)}$	O3h	IO	-	mmol Eq m ⁻³	Total Alkalinity
$P_i^{(1)}$	P1[cnpslf]	LO	C N P Si Chl Fe	mg C m ⁻³ , mmol N-P-Si m ⁻³ , mg Chl- <i>a</i> m ⁻³ , μ mol Fe m ⁻³	Diatoms
$P_i^{(2)}$	P2[cnplf]	LO	C N P Chl Fe	mg C m ⁻³ , mmol N-P m ⁻³ , mg Chl- <i>a</i> m ⁻³ , μ mol Fe m ⁻³	NanoFlagellates
$P_i^{(3)}$	P3[cnplf]	LO	C N P Chl Fe	mg C m ⁻³ , mmol N-P m ⁻³ , mg Chl- <i>a</i> m ⁻³ , μ mol Fe m ⁻³	Picophytoplankton
$P_i^{(4)}$	P4[cnplf]	LO	C N P Chl Fe	mg C m ⁻³ , mmol N-P m ⁻³ , mg Chl- <i>a</i> m ⁻³ , μ mol Fe m ⁻³	Large phytoplankton
B_i	B1[cnp]	LO	C N P	mg C m ⁻³ , mmol N-P m ⁻³	Pelagic Bacteria
$Z_i^{(3)}$	Z3[cnp]	LO	C N P	mg C m ⁻³ , mmol N-P m ⁻³	Carnivorous Mesozooplankton
$Z_i^{(4)}$	Z4[cnp]	LO	C N P	mg C m ⁻³ , mmol N-P m ⁻³	Omnivorous Mesozooplankton
$Z_i^{(5)}$	Z5[cnp]	LO	C N P	mg C m ⁻³ , mmol N-P m ⁻³	Microzooplankton
$Z_i^{(6)}$	Z6[cnp]	LO	C N P	mg C m ⁻³ , mmol N-P m ⁻³	Heterotrophic Flagellates
$R_i^{(1)}$	R1[cnpf]	NO	C N P Fe	mg C m ⁻³ , mmol N-P m ⁻³ , μ mol Fe m ⁻³	Labile Dissolved Organic Matter
$R_c^{(2)}$	R2c	NO	C	mg C m ⁻³	Semi-labile Dissolved Organic Carbon
$R_i^{(3)}$	R3c	NO	C	mg C m ⁻³	Semi-refractory Dissolved Organic Carbon
$R_i^{(6)}$	R6[cnpsf]	NO	C N P Si Fe	mg C m ⁻³ , mmol N-P-Si m ⁻³ , μ mol Fe m ⁻³	Particulate Organic Detritus

Table 4.2: List of the reference state variables for the pelagic model. Type legend: IO = Inorganic; LO =Living organic; NO=Non-living organic. The subscript i indicates the basic components (if any) of the variable

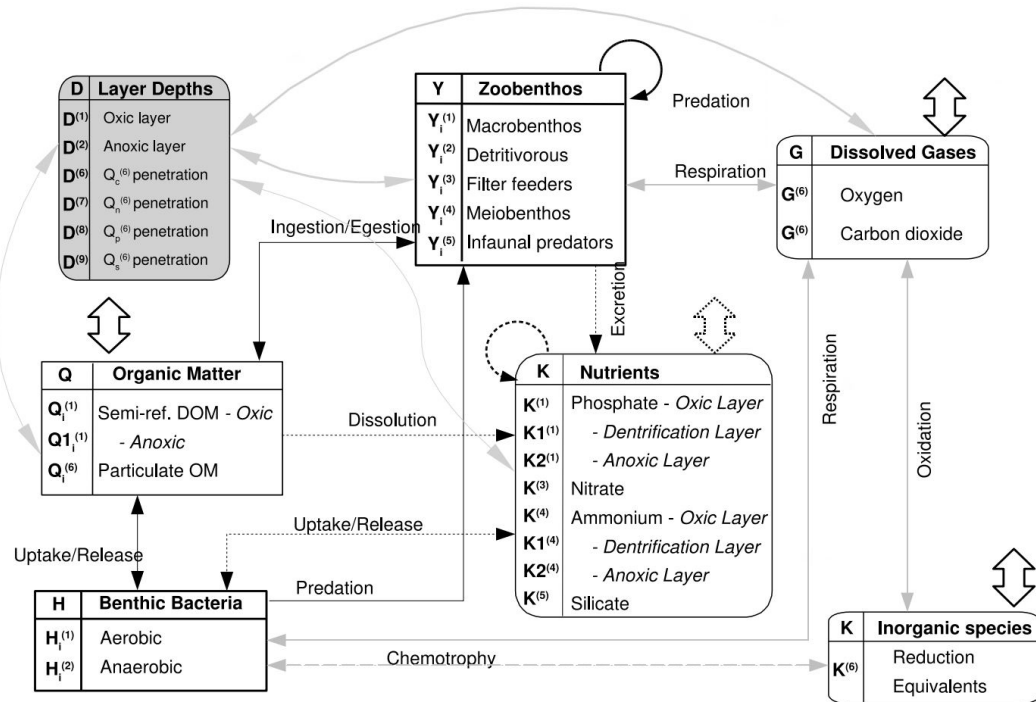


Figure 4.3: BFM benthic system representation. Image taken by Vichi et al. (2006)

4.2.3 Benthic model

This section describes the equations for the benthic model (Figure 4.3) using the mathematical formulation defined for the pelagic model. The pelagic and the benthic systems are connected each other through the water-sediment interface, which is located at depth $z = -H$ in the pelagic system of coordinates, where H is the bottom depth.

Fluxes are considered positive downwards, and the fluxes from the benthic to the pelagic system are negative.

The main processes considered in the benthic model are:

- deposition and incorporation of particulate organic matters from the pelagic system;
- cycling of carbon and nutrients through the benthic food web;
- early-diagenesis (oxic and anoxic mineralization)
- flux exchanges of dissolved (in)organic compounds at the sediment-water interface

4.2 BFM: Biogeochemical Flux Model

- resuspension processes is not included in the original model, but are now considered and described in section 4.4.

As it is, the generic equations for the benthic variables do not have any physical transport term, but only biogeochemical source and sink terms.

The BFM benthic model is essentially a layer model in which the concentrations of the LFGs and CFFs are treated as bulk values in the sediment. Therefore, the units of the state variables are given per $[m^{-2}]$. All the variables of the BFM benthic model are reported in the Table 4.3. Like for the pelagic case is reported a bravely description of the system.

The functional groups are essentially 3-dimensional vectors with only the C, N and P components.

The system is characterized by 5 LFGs those are: epifaunal predators Y_i^1 ; Deposit feeders Y_i^2 : all the organisms whose diet consists of benthic detritus and smaller organisms; Filter feeders Y_i^3 : organisms that feeds directly from the pelagic system by filtering the suspended particles; Meiobenthos Y_i^4 : protozoa and animals with a small impact on the sediment distribution: main predators of benthic bacteria; Infaunal predators Y_i^5 .

Two different groups of microbial decomposers are considered: aerobic bacteria $H_i^{(1)}$ (a large group of decomposers that needs oxygen for their functional dynamics); anaerobic bacteria $H_i^{(2)}$ (which combines the functionality of both the nitrate and sulphate reducers).

The fluxes which determine the benthic organisms concentration are generated by different processes. They could be summed with some equation. As done for the pelagic model, we will refer to the generic groups Y and H :

$$\begin{aligned} \frac{\partial Y}{\partial t} \Big|_{bio} &= \frac{\partial Y}{\partial t} \Big|_{ing} - \frac{\partial Y}{\partial t} \Big|_{resp} - \frac{\partial Y}{\partial t} \Big|_{rel} - \frac{\partial Y}{\partial t} \Big|_{pred} ; \\ \frac{\partial H}{\partial t} \Big|_{bio} &= \frac{\partial H}{\partial t} \Big|_{upt} - \frac{\partial H}{\partial t} \Big|_{resp} - \frac{\partial H}{\partial t} \Big|_{rel} - \frac{\partial H}{\partial t} \Big|_{pred} . \end{aligned} \tag{4.9}$$

All the groups also indulge in cannibalism (included in the equation), because these fluxes stabilize the oscillations of the functional group dynamics (Vichi et al.

(2006)).

Benthic organism physiology is supposed to be affected by the water temperature (we assume sediments are in a thermal equilibrium with the water) with the same form of the regulating factor as presented in the pelagic model (Equation 4.7).

Benthic-pelagic coupling

The pelagic and the benthic systems are connected each other through the water-sediment interface, which is located at depth $z = -H$ in the pelagic system of coordinates.

This coupling is the principal feature of interests for this study. In particular, the fluxes of organic matter between the two layers: $R6c$ (SSC) \leftrightarrow $Q6c$ (Detritus). Basic condition is the use of a simple benthic return model for the benthic closure. In order to parameterise the benthic re-mineralisation, a fixed quota of each detritus component (C, N, P, Si) reaching the bottom is returned to the water column as nutrients.

Nutrient fluxes

The diffusive fluxes from the sediment to the water column is defined as follow:

$$\begin{aligned} \frac{\partial K_i}{\partial t} \Big|_{diff}^{N_i} &= -r_i K_i \\ \frac{\partial N_i}{\partial t} \Big|_{diff}^{K_i} &= - \frac{\partial K_i}{\partial t} \Big|_{diff}^{K_i} \cdot \frac{1}{\Delta z} \end{aligned} \quad (4.10)$$

where

- K_i = nutrient concentration in the sediment $[\frac{mmol}{m^2}]$;
- N_i = nutrient concentration in the water column $[\frac{mmol}{m^3}]$;
- r_i = diffusive time scale $[d^{-1}]$;
- Δz = thickness of the bottom box $[m]$.

4.2 BFM: Biogeochemical Flux Model

Deposition

The main input to benthic system is the sedimentation of particles from the water column enters into the organic matter pools of the sediments ($Q_i^{(6)}$ and $Q_i^{(1)}$). This parametrization, in the standard model, is done imposing a constant sinking velocity of the SSC ($w_s = -1.5m/day \approx 1.22 \cdot 10^{-3}m/s$) and a deposition advective flux calculated in the follow way at the bottom:

$$\left. \frac{\partial Q_i^{(6)}}{\partial t} \right|_{sed}^{R_i^{(6)}} = w_s^b R_i^{(6)} \Big|_{z=-H} \quad (4.11)$$

where $R_i^{(6)}$ is the concentration of SSM [$mmol/m^3$], the subscript represents the constituent.

This sedimentation flux crossing every layer of the water column.

In section 4.4 it is described the newly implemented organic matter deposition/resuspension model.

Variable	Type	Constituent	Description	Reference
$K^{(1)}$	CFE	P	Phosphate in oxic layer (mmol P m ⁻²)	Ruardij and Van Raaphorst, 1995
$K_1^{(1)}$	OSV	P	Phosphate in denitrification layer (mmol P m ⁻²)	“
$K_2^{(1)}$	OSV	P	Phosphate in anoxic layer (mmol P m ⁻²)	“
$K^{(3)}$	OSV	N	Nitrate in the sediments (mmol N m ⁻²)	“
$K^{(4)}$	OSV	N	Ammonium in oxic layer (mmol N m ⁻²)	“
$K_1^{(4)}$	OSV	N	Ammonium in denitrification layer (mmol N m ⁻²)	“
$K_2^{(4)}$	OSV	N	Ammonium in anoxic layer (mmol N m ⁻²)	“
$K^{(5)}$	OSV	Si	Silicate in the sediments (mmol Si m ⁻²)	“
$K^{(6)}$	OSV	R	Reduction equivalents, Fe(II), Mn(II), HS ⁻ (mmol S m ⁻²)	“
$G^{(2)}$	OSV	O	Dissolved Oxygen (O ₂) in oxic layer (mmol O ₂ m ⁻²)	Ebenhoeh et al, 1995; Ruardij and Van Raaphorst, 1995
$G^{(3)}$	OSV	C	Dissolved CO ₂ in the sediments (mg C m ⁻³)	“
$Y_i^{(1)}$	LFG	C N P	Epibenthic Predators (<i>megabenthos</i>) (mg C m ⁻² or mmol nut. m ⁻²)	Ebenhoeh et al, 1995; Blackford, 1997
$Y_i^{(2)}$	LFG	C N P	Deposit Feeders (“)	“
$Y_j^{(3)}$	LFG	C N P	Filter Feeders (“)	“
$Y_j^{(4)}$	LFG	C N P	Meiobenthos	“
$Y_j^{(5)}$	FG	C N P	Infaunal Predators (“)	“
$H_j^{(1)}$	FG	C N P	Aerobic Benthic Bacteria (“)	“
$H_j^{(2)}$	FG	C N P	Anaerobic Benthic Bacteria (“)	“
$D^{(1)}$	OSV	-	Oxic layer depth (m)	Ruardij and Van Raaphorst, 1995
$D^{(2)}$	OSV	-	Sulfide horizon depth (m)	“
$D^{(6)}$	OSV	-	Average penetration depth for the C-component in detritus (m)	Ebenhoeh et al, 1995
$D^{(7)}$	OSV	-	As above, but for the N-component	“
$D^{(8)}$	OSV	-	As above, but for the P-component	“
$D^{(9)}$	OSV	-	As above, but for the Si-component	“
$Q_i^{(1)}$	OSV	C N P	Dissolved Organic Matter in the oxic layer (mg C m ⁻² or mmol nut. m ⁻²)	-
$Q_i^{(1)}$	OSV	C N P	Dissolved Organic Matter in the anoxic layer (“)	-
$Q_i^{(6)}$	OSV	C N P Si	Particulate Organic Detritus in the sediments (“)	Ebenhoeh et al, 1995; Ruardij and Van Raaphorst, 1995

Table 4.3: List of the reference state variables for the benthic model. The subscript j indicates the basic components (if any) of the variable

4.3 The transport model

The transport equation is given by Equation 4.27. To solve that is used the same scheme of the POM integration. The transport of the biological state vector, in discrete form, is:

$$c_{n+1} = \tilde{c} + Diff(c_{n+1})2\delta t \quad (4.12)$$

$$\tilde{c}^k = c_{n-1}^k + \frac{1}{2\delta\sigma} [(c_n^{k-1} + c_n^k) w^k - (c_n^k + c_n^{k+1}) w^{k+1}] 2\delta t \quad (4.13)$$

where k stays for the vertical level, n to the time level, $\delta\sigma$ is the cell thickness (σ -coordinates), $Diff$ is a shorthand for the spatial discretization of the implicit diffusion term.

4.4 The sediment deposition/resuspension model

The sediment deposition/resuspension submodel has been inserted into the 1D POM-BFM model by introducing a modification of the Wang and Pinardi (2002) procedure that allows the computation of the combined current and wave effect on the bottom stress.

This section describes the submodel implemented. For convenience, in the following, two different stresses are defined:

$\tau_{bm} \equiv \tau_b$ is the mean bottom stress;

τ_{bmax} is the maximum bottom stress.

The first one is the mean stress already defined in chapter 2 and section 4.1, which is used by the model for the calculation of the velocity profile and the kinetic energy. The second one is the maximum stress which has to be computed for defining the resuspension process.

4.4.1 Particulate organic matter flux calculation at the sediment-water interface

The variation of the concentration of the particulate organic matter (POM) is regulated by the advective and diffusive terms already seen in section 4.1 for the physical rate of change (Equation 4.27).

$$\frac{\partial C}{\partial t} + (w + w_s) \frac{\partial C}{\partial z} = \frac{\partial}{\partial z} \left(K_v \frac{\partial C}{\partial z} \right)$$

where C is the POM concentration [$mg\ m^{-3}$], w is the fluid vertical velocity, w_s the POM sinking velocity (compared to the fluid) and K_v the turbulent viscosity.

The feature of this deposition/resuspension submodel is to modify the bottom boundary conditions seen in Equation 4.11, which considers only the deposition process, introducing also the resuspension process.

With this configuration, the POM bottom boundary condition is defined according to

$$K_v \frac{\partial C}{\partial z} \Big|_{z=-H} = S$$

4.4 The sediment deposition/resuspension model

where S is the flux of the sediments from/to ocean to/from benthic domain due to deposition ($S < 0$) or resuspension ($S > 0$).

These fluxes, in the model, are quantified according to Ariathurai and Krone (1976) assuming proportionally with the bottom stress:

$$\begin{cases} S = S_0 \left(\frac{|\tau_{bmax}|}{\tau_{crit}} - 1 \right) & \text{if } |\tau_{bmax}| \geq \tau_{crit} \\ S = C_b w_{dep} \left(\frac{|\tau_{bmax}|}{\tau_{crit}} - 1 \right) & \text{if } |\tau_{bmax}| < \tau_{crit} \end{cases} \quad (4.14)$$

where C_b is the POM concentration at the bottom layer; w_{dep} is the deposition velocity that has the value of the sinking velocity w_s with a saturation value w_{bur} : $w_{dep} = \max\{w_s; w_{bur}\}$;

w_s and τ_{crit} are respectively the deposition velocity of the POM and the critical stress, which are defined above;

S_0 is the maximum resuspension flux depending on the benthic sediment concentration and on the resuspension velocity w_{res} :

$$S_0 = \frac{C_{ben}}{\Delta ben} w_{res} \quad (4.15)$$

where Δben is the thickness of the benthic sediments deposit, C_{ben} is the concentration per m^2 of the sediments [$mg\ m^{-2}$] and w_{res} has the value of $10^{-7}\ m\ s^{-1}$. The mean value of the S_0 is of the order of $10^{-6}mg\ m^{-2}\ s^{-1}$.

Also the modulating part (terms within the brackets in Equation 4.14), depending on the rate τ_{bmax}/τ_c , is important. This makes the two fluxes converging to zero at the threshold value τ_{crit} .

A correction of the parametrization of the resuspension flux, defined by the Equation 4.14, has been done in order to consider a resuspension flux saturation value. In this way S_0 is considered the maximum resuspension flux and the equation is modified as follow:

$$\begin{cases} S = S_0 (mod - 1) \cdot \frac{1}{rate-1} & \text{if } |\tau_{bmax}| \geq \tau_{crit} \\ S = C_b w_{dep} \left(\frac{|\tau_{bmax}|}{\tau_{crit}} - 1 \right) & \text{if } |\tau_{bmax}| < \tau_{crit} \end{cases} \quad (4.16)$$

where

$$mod = \min \left\{ \frac{|\tau_{bmax}|}{\tau_{crit}}; rate \right\};$$

$rate > 1$ defines the value of saturation of the rate $|\tau_{bmax}|/\tau_{crit}$ over that the flux remains constant at S_0 . In this work $rate = 2$.

Finally the sinking velocity w_s and the critical stress τ_c are defined merging to the Stokes law and the Shields function as in Wang and Pinardi (2002):

$$w_s = \frac{gd^2}{18\nu} \left(\frac{\rho_s}{\rho_w} - 1 \right) \quad (4.17)$$

$$\tau_{crit} = \rho_w \left[\frac{g(\rho_s - \rho_w)\nu}{10\rho_w} \right]^{2/3} \quad (4.18)$$

where:

ρ_s is the density of the particulate in the benthic;

ν is the molecular kinematic viscosity;

d is the diameter of the sediments.

Phytoplankton flux calculation at the sediment-water interface

Similar approach is used for the parametrization of the deposition of the Phytoplankton. As seen for the POM, the deposition is a net flux of Phytoplankton to benthic detritus (Q^6 and Q^1 : see Figure 4.3). Therefore there is not phytoplankton resuspension, but when τ_{bmax} exceeds the τ_{crit} value the bottom phytoplankton deposition is interrupted. The phytoplankton deposition process is therefore calculated as follow:

$$\begin{cases} S = 0 & \text{if } |\tau_{bmax}| \geq \tau_{crit} \\ S = P_b w_{dep}^{phyto} \left(\frac{|\tau_{bmax}|}{\tau_{crit}} - 1 \right) & \text{if } |\tau_{bmax}| < \tau_{crit} \end{cases} \quad (4.19)$$

where P_b is the phytoplankton concentration at the bottom layer and w_{dep}^{phyto} is the deposition velocity of the phytoplankton. This velocity is regulated according to the nutrient stress conditions according to:

$$\tilde{w}_{dep}^{phyto} = w_{max}^{sink} \cdot \max \{0, l^{sink} - f^{nut}\} \quad (4.20)$$

where w_{max}^{sink} is the maximum sedimentation rate, f^{nut} is the term regulating the phytoplankton nutrient stress ($0 \leq f^{nut} < 1$) and $l^{sink} = 0.75$.

However at the sediment-water interface the phytoplankton sinking velocity (w_{dep}^{phyto}) cannot exceed the prescribed velocity w_{bur}^{phyto} : $w_{dep}^{phyto} = \max \{ \tilde{w}_{dep}^{phyto} ; w_{bur}^{phyto} \}$.

4.4 The sediment deposition/resuspension model

4.4.2 Stresses calculation

The new definition of the bottom stress has the main aim of combine the current and wave components in a unique stress, while before was considered only the stress due to the wind-driven current. The stress depending on such two components is defined according to Grant and Madsen (1979); Lou et al. (2000):

Mean current bottom stress

The first step is to define the drag coefficient of the bottom shear stress. The formulation used is the same of the POM1D (Equation 4.3) through the Wall-law.

Using the closure of the turbulence (chapter 2), C_d links the bottom stress to the mean current velocity as follow:

$$\tau_b = \tau_c = \rho C_d |u_c| u_c \quad (4.21)$$

where τ_c indicates the bottom stress due to the mean current.

In case of no wave motion $\tau_{bmax} = \tau_{bm} = \tau_c$.

This parametrization is obtained considering a turbulent regime (easily verified in the oceanic PBL), as already explained in section 4.1

Wave bottom stress

The surface waves generate an orbital motion propagating downward in the water column. The orbital (oscillating) velocity produces the bottom stress of the column, that can be larger than the mean current bottom stress. This stress is proportional to the maximum near bottom wave orbital velocity u_w , which could computed using the linear wave theory . Knowing the period T and the significant height h_s of the surface waves, is possible to define u_w :

$$|u_w| = \frac{1}{2} \frac{h_s \omega}{\sinh(kH)}$$

where $\omega = 2\pi/T$ is the angular frequency and k the wave number.

The wave number is calculated with a second equation based on the wave linear theory:

$$\omega^2 = gk \tanh(kH)$$

That is done leading to convergence the homogeneous equation

$$gk \tanh(kH) - \omega^2 = 0$$

starting with two boundary values

$$\begin{cases} k_1 = 2\pi \\ k_2 = 2\pi/1000 \end{cases}$$

Wave bottom stress - τ_w

The stress due to the wave motion is proportional to the orbital velocity u_w and to the wave friction coefficient f_w in the form:

$$\tau_w = \rho u_{*w}^2 = \frac{1}{2} \rho f_w u_w^2 \quad (4.22)$$

where u_{*w}^2 is wave friction velocity.

The definition of f_w can be done in different ways based on the wave regime and on the seabed characteristics (rough or smooth).

Wave-current interaction

The presence of u_w at the bottom increases the turbulence in the bottom layer. This generates an additional friction that has to be combined with the friction due to current motion. An important contribution to the definition of the wave-current interaction is due to Grant and Madsen who have published many of their studies (see Grant and Madsen (1979)).

The computation of the amplitude of the stress defined in that work and used in Wang and Pinardi (2002) is done through a quadratic law:

$$\tau_{bmax} = \frac{1}{2} \rho f_{cw} |u_c + u_w|^2 \quad (4.23)$$

where u_w is the maximum near bottom wave orbital velocity determined from linear wave theory and f_{cw} is the effective friction coefficient. This is calculated through a convergence method well explained in Lou et al. (2000).

For the Equation 4.23 definition u_c and u_w are assumed to have the same direction.

4.4 The sediment deposition/resuspension model

In Wang and Pinardi (2002) is use a semi-empirical parametrization of the stress coupling introduce by Grant and Madsen (1979). This formulation needs the comparability of the two velocities due to mean circulation (u_c) and to the wave motion (u_w). This condition isn't often verified in the results of the implementation of the model here analyzed. The consequence is the underestimation of the maximum bottom stress.

For this reason, a different parametrization of the combined stress has been considered. For simplicity of calculation, a formula known as DATA2 method has been utilized. Soulsby proposed it in 1995 (Soulsby (1995)) as a direct fit to 61 laboratory measurements and 70 field measurements of the cycle-mean bed shear-stress τ_{bm} (all for rough beds).

The DATA2 formulation is:

$$\tau_{bm} = \tau_c \left[1 + 1.2 \left(\frac{\tau_w}{\tau_c + \tau_w} \right)^{3.2} \right] \quad (4.24)$$

where τ_c and τ_w are the two bottom stress generated respectively by the current and the wave motion alone.

While the maximum bottom stress is given by:

$$\tau_{bmax} = \sqrt{[(\tau_m + \tau_w |\cos\phi|)^2 + (\tau_w |\sin\phi|)^2]} \quad (4.25a)$$

$$\xrightarrow{\phi=0} \tau_m + \tau_w \quad (4.25b)$$

where ϕ is the angle through the two velocities considered null as for Equation 4.23.

4.5 Coupling

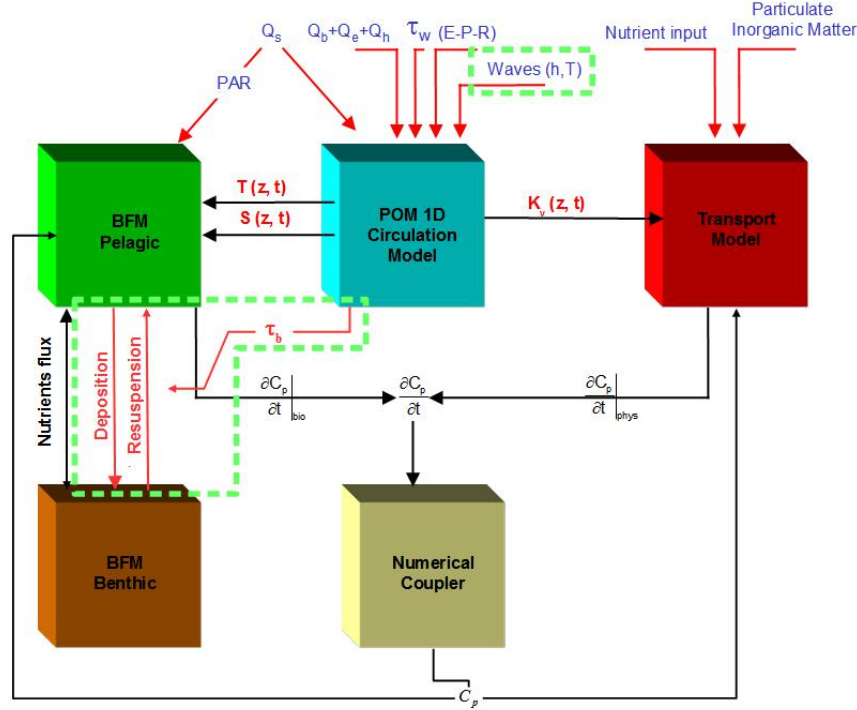


Figure 4.4: Model's blocks and their interactions. The green dotted shapes shown the corrections done by the deposition/resuspension submodel.

The partition of the model in two different submodels imposes a separate calculation of physical biological time rate of change of the state variables (Figure 4.4). These two rates are then merged in a single one. At each time step a generic biogeochemical state variable C is computed (integrated) by solving the equation

$$C_{n+1} = C_n + \int_{t_n}^{t_{n+1}} \left(\left. \frac{\partial C}{\partial t} \right|_{phys} + \left. \frac{\partial C}{\partial t} \right|_{bio} \right) dt \quad (4.26)$$

where the subscript indicates the time step t_n .

The $\left. \frac{\partial C}{\partial t} \right|_{bio}$ contains the changing rates of the state vector due to biogeochemical processes.

The physical rate is solved like follow:

$$\left. \frac{\partial C}{\partial t} \right|_{phys} = -Advection + Diffusion = -w_s \frac{\partial C}{\partial z} + \frac{\partial}{\partial z} \left(\nu_{turb} \frac{\partial C}{\partial z} \right) \quad (4.27)$$

where w_s is the sinking velocity and ν_{turb} the turbulent viscosity.

4.5 Coupling

The scheme used in the model for the integration is the Leap Frog scheme:

$$C_{n+1} = C_{n-1} + S(C_n) \delta t$$

an explicit two-step scheme of second order, where S is the particular process which generate a rate change. Well known stability issues due to uncoupling of odd and even integration steps impose to use a numerical filter: Asselin-filter (Asselin (1972)):

$$F_{C_n} = C_n + \frac{\alpha}{2} (C_{n-1} - 2C_n + C_{n+1})$$

with $\alpha = 0.3$.

Every blocks work separately and communicate through the outputs/inputs. A scheme of the interactions is shown in the Figure 4.4.

The physical model is forced by heat ($Q_s+Q_b+Q_h+Q_e$), water ($E-P-R$; evaporation, precipitation, riverine input) and momentum (wind stress, τ_w) fluxes, and computes vertical profiles of temperature (T), salinity (S) and turbulent diffusivity ($\nu = \nu_{turb}$). The temperature and salinity fields are passed to the biogeochemical model for the computation of the metabolic response of the biota and the oxygen saturation concentration. The turbulent diffusivity is passed to the transport model for the computation of $\frac{\partial C}{\partial t}|_{phys}$.

However, as specified in section 5.2, in this implementation the temperature and the salinity vertical profile are prescribed by data (monthly varying climatologies). The biogeochemical model is forced by solar radiation (Q_s), expressed as photosynthetically available radiation (PAR, about 50% of the incoming solar radiations flux) and computes $\frac{\partial C}{\partial t}|_{bio}$.

The coupling of the system occurs at the level of the numerical coupler, which merges the two rates according to the characteristics of the coupling method used.

The coupling is numerically carried out by applying the *Source Splitting* technique (Butenschön et al. (2012), Butenschön (2007)) and in particular the technique described below.

4.5.1 Source Splitting

The *Source Splitting* mechanism is based on the separation of the two process's integration in two different time step: the slower of the two involved processes is considered constant on a certain coarse time interval while the finer integration time step is imposed by the faster process.

In this model the time step is imposed by the physical processes while the biogeochemical processes are assumed to be the slower. The global integration step (δt_{glob}) is expressed as:

$$C_{n+1} = C_n + \int_{\delta t_{glob}} \left. \frac{\partial C}{\partial t} \right|_{phys} dt + \left. \frac{\partial \tilde{C}}{\partial t} \right|_{bio} \delta t_{glob} \quad (4.28)$$

The change rate due to the biogeochemical processes is calculated after a time step $\delta t_{est} > \delta t_{glob}$ (external) with the semi-implicit equation

$$\left. \frac{\partial C(\tilde{t}_{n+s})}{\partial t} \right|_{bio} = \left. \frac{\partial C(t_n)}{\partial t} \right|_{bio} + \frac{\left. \frac{\partial C(t_n)}{\partial t} \right|_{bio} - \left. \frac{\partial C(t_n - \delta t_{est})}{\partial t} \right|_{bio}}{\delta t_{est}} \cdot (t_{n+s} - t_n), \quad (4.29)$$

where s represents the middle steps.

In this case $\delta t_{glob} = 864s$ (100 step per day) and $\delta t_{est} = 2\delta t_{glob}$.

Chapter 5

Implementation

5.1 Adriatic Sea

The Adriatic Sea (Figure 5.1) is an elongated semi-enclosed basin, approximately 800 km long and 200 km wide with an area of 160,000 km^2 . It consists of a shallow northern shelf, with a depression of 270 m in the middle basin (Jabuka Pit), and a deep southern part with a maximum depth of 1320 m. On the western coast of the Adriatic Sea, the shelf has a gradual slope with isobaths running parallel to the coastline. The eastern coast is irregular, and composed of many islands with steeper continental shelf breaks.

The Po River is the main freshwater source, providing up to 50 % of total river runoff. The Po River discharges at an annual average rate of $1500m^3s^{-1}$.

The area is characterized by strong northeasterly winds during winter (Bora) (Signell et al. (2010)), while during summer and autumn winds could be southeasterly with smaller amplitude (Scirocco) (??). These strong winds have the capacity to generate important wave regimes in the NAS. Such a surface motion strongly influences the dynamics of the sea at different depths, increasing the turbulent energy. In a shallow water geometry like that of the NAS, the bottom layer is affected by an intensification of the Benthic Boundary Layer.

The general circulation of the Adriatic Sea is cyclonic and highly variable with seasons (Zavatarelli et al., 2002; Zavatarelli and Pinardi, 2003; Pullen et al., 2003). One of the major features is a coastal current along the western side of the basin, the Western Adriatic Coastal Current (WACC), driven by wind and thermohaline forcing. The WACC reaches maximum amplitude during winter due to the strong

Bora wind energy input. The thermohaline structure of the WACC is connected to the Po River fresh water river runoff and winter surface heat loss in the NAS (Raicich, 1996; Kourafalou, 1999; Wang, 2005).

The Gulf of Trieste (GoT) is a small-scale (approximately $25\text{km} \times 325\text{km}$ wide) and shallow (maximum depth $\approx 38\text{m}$) basin located in the northeastern corner of the NAS to which it is connected through its western side. The GoT can be classified as a region of freshwater influence since the circulation in the area responds to a number of complex processes controlled by tides, wind, waves, and variations in river discharge that significantly vary on a year-to-year time scale. A persistent freshwater tongue originating from the Isonzo-Soča river outflow constitutes the major freshwater input in the area and characterizes surface outflow



Figure 5.2: Representation of the Gulf of Trieste and its main circulation. Image taken from Cosoli et al. (2013).

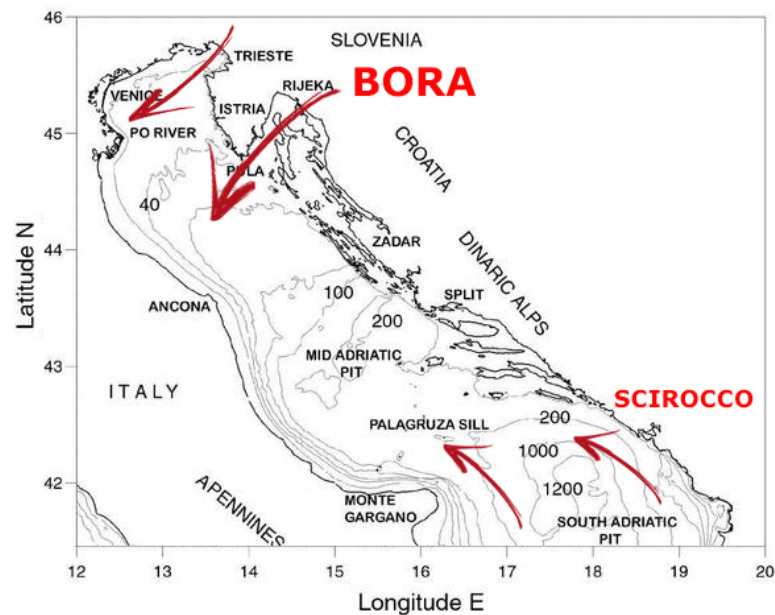


Figure 5.1: Adriatic sea bathymetry; Bora and Scirocco locations.

5.1 Adriatic Sea

along the Italian coastline in the northern flank. Several studies have also shown that the Po river may also impact the freshwater input in the GoT during summer and autumn (Malacic and Petelin (2009)).

Circulation is a gyre-type circulation pattern with a weak ($2 - 3\text{cm/s}$) permanent cyclonic (counterclockwise) circulation in the bottom layer (below 10m depth), and an alternating, wind-driven, cyclonic (anticyclonic) flow in the surface (approximately 5m thick) layer. Tidal oscillations in the Adriatic Sea originate primarily from remote forcing in the Ionian and Mediterranean seas and enter the Adriatic basin through the Otranto strait.

The basin-wide circulation in the GoT is mainly driven by meteorological forcing, especially by the cold "Bora" and, to a minor extent, by the warmer "Sirocco" wind during windy seasons (mostly fall and winter), and by thermohaline processes during summer. The stress produced by the combination of the mean circulation and wave motion determines the interaction between the water motion and the benthic sediments.

In the NAS, two main classes of sediments can be identified (Wang et al. (2007)). The first class consists of coarser sediments of sand with grain size between 50 and 2000mm . The second class is of finer materials of silt with grain size between 2 and 50mm . It has long been recognized that the fine sediments such as fine sand, silt and clay are mainly supplied from the NAS rivers, and transported southward by the coastal current. The sediments imported by the rivers contain different elements really important for the biogeochemical cycle of the sea.

5.2 Data inputs

The model implementation is in accordance with Mussap et al. (2016), which is relative to the area with the code-numbered *MA21* situated in the center of the GoT and shown in Figure 5.3. Monitoring data for the whole area were used to set initial conditions, surface boundary conditions, and to validate the model's performance.

In the following a brief description of the implementation is given.

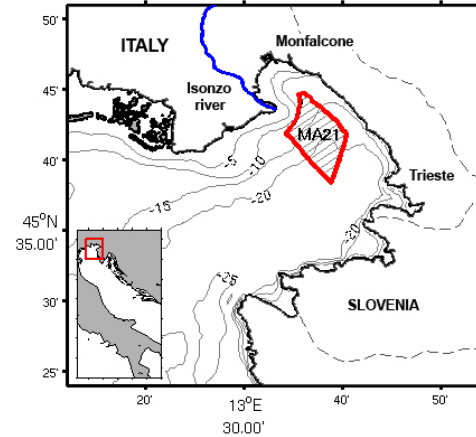


Figure 5.3: Localization of the simulated area. Image taken from Mussap et al. (2015).

Vertical profile

The vertical profile of the model is subdivided in 30 layers with different thickness, as explained in section 4.1. The column of water is 16m deep.

Temperature and salinity

The hydrological data, temperature and salinity vertical profiles, used to compose the prescribed climatology, originate from the monitoring activities carried out in the Gulf of Trieste by ARPA-FVG and OGS from 2000 to 2013 (Mussap et al. (2015)). From such data sets, climatological temperature and salinity monthly profiles have been computed and provided to the model via linear interpolation between adjacent values.

The climatological annual cycles of the temperature and salinity are shown in Figures 5.4a and 5.4b, respectively. They show a seasonal cycle characterized by well-mixed conditions in the winter and by vertical thermal stratification in the summer. Surface salinity is effected by pulses of freshwater originating from the rivers, while below the surface there are periodical increases in the salinity value. Using this data the POM model calculates also the annual cycle of density of the water column shown in Figure 5.4c.

5.2 Data inputs

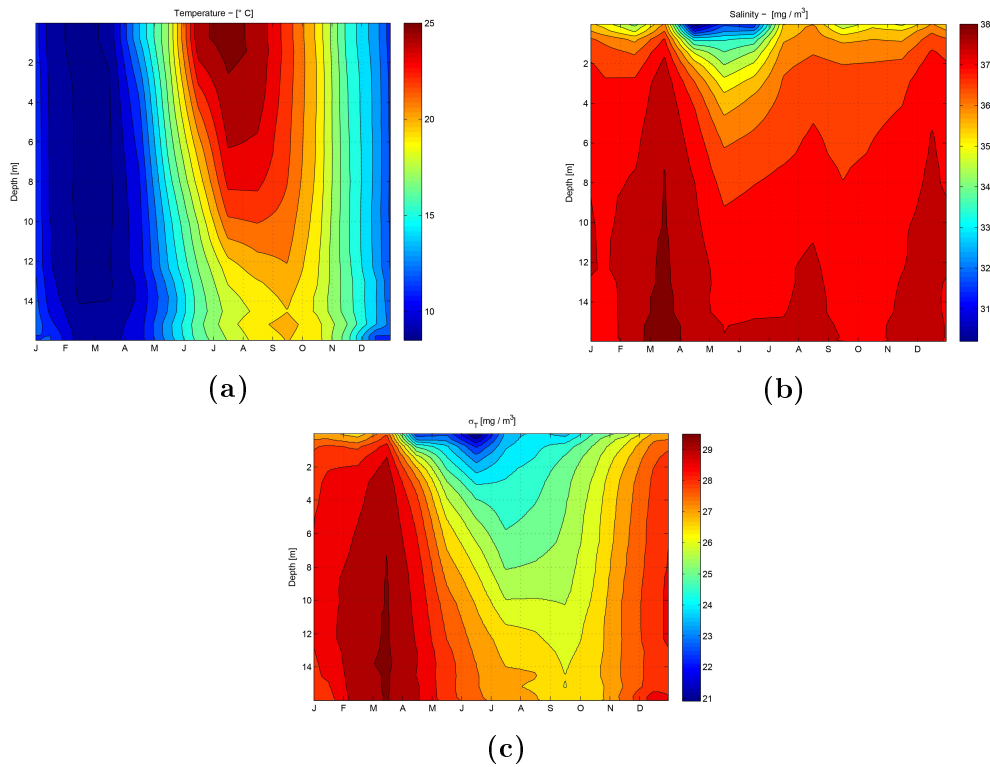


Figure 5.4: Temperature (a), salinity (b) monthly climatological profiles calculated from available in situ data fed to the model and interpolated on its time step. From this value is calculated also the density (c), which is reported as $\sigma_T = Den - 1000$.

Wind and radiation

The surface wind stress is the only surface forcing function.

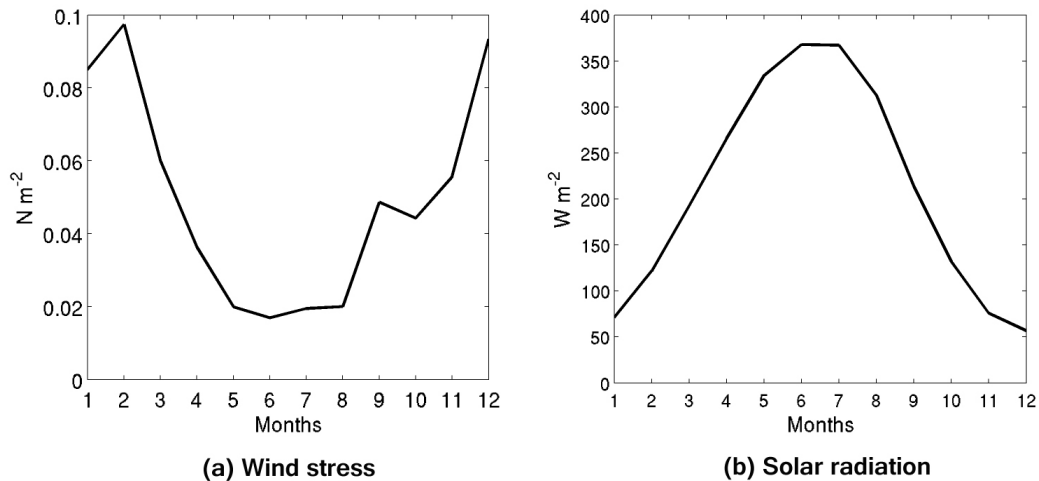


Figure 5.5: Wind stress (a) and radiation (b) forcing input at the surface.

The annual, monthly varying, climatology used here was obtained from the 6-hour ECMWF ERA-interim reanalysis (Berrisford et al., 2009) relative to 2000-

2013 (Figure 4A and Table 1).

Wind stress is highest during winter and autumn, reflecting the prevalence of the typical strong Bora (northeasterly) and Scirocco (south-easterly) winds, respectively (Kourafalou, 1999; Zavatarelli et al., 2002). Winds are weaker during spring and summer. The daily surface incident shortwave radiation also originates from the ECMWF data (Figure 5.5) which are of the same form as the wind's one.

5.3 Waves

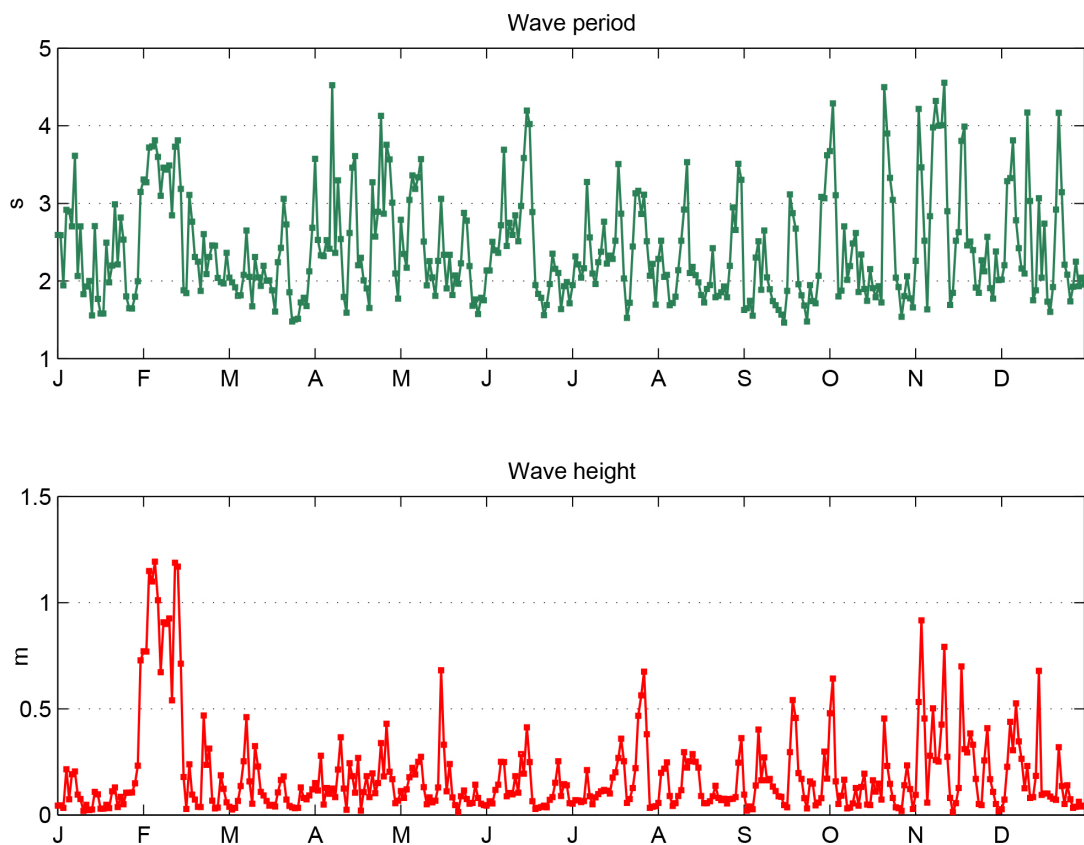


Figure 5.6: The waves mean period (top) and height (bottom) computed with the climatological model NEMO-WW3. The more important heights persist in February and for several days, while the periods oscillate with not particular events.

The wave data originates from simulations carried out with the coupled 3D general circulation wave model NEMO-WW3 (WaveWatchIII) implemented in the Mediterranean sea (Clementi, E. (2013)). From the simulated Mediterranean Sea 2012 wave field the daily values for the Gulf of Trieste data were extracted

5.4 Bottom stress

and used to compute the wave dependent bottom shear stress for the deposition/resuspension model.

The relevant wave data are the wave period (T) and the significant height (h_s). The yearly cycle of the observed wave properties is plotted in Figure 5.6.

5.4 Bottom stress

For the definition of the sinking velocity w_s and the threshold stress τ_{crit} , defined in section 4.4, are considered the parameters used by Wang and Pinardi (2002), where:

$\rho_s = 1100 \text{ mg m}^{-3}$ is the density of the particulate in the benthic;

the molecular kinematic viscosity is $\nu = 1.3 \cdot 10^{-6} \text{ m}^2 \text{ s}^{-1}$;

the diameter of the sediments for fine sand and silt have a diameter $20 < d < 60 \mu \text{ m}$. In this work is taken a diameter of $24 \mu \text{ m}$ in order to obtaining $w_s \approx 1.5 \text{ m d}^{-1}$, as like as the basic model.

τ_{crit} has been fixed at $0.02 \text{ mg m}^{-1} \text{ s}^{-2}$. This is a good approximation generated substituting the mean values of ρ_w in the critical stress formulation (Equation 4.18).

These values are within ranges of those used by other researchers [e.g., Clarke and Elliot (1998); Chao (1998)].

5.5 Experiments definition

The following numerical experiments were carried out (see also Table 5.1).

Case	$t_{storm(day)}$	Position	Peak
Original	no waves	no Resuspension	no Resuspension
Base	no waves	/	/
BaseW	no storm	/	/
W1	12	BP	
W2	25	DP	I
W3	38	AP	
W4	230	BP	
W5	250	DP	II
W6	272	AP	
W7	320	BP	
W8	330	DP	III
W9	340	AP	

Table 5.1: Cases of experiments done. Every event is imposed from the third year at the day shown in table and lasts for 10 days. The third column indicates the position of the storm respect the referent peak: BP=Before Peak; DP=During Peak AP=After Peak. See Figure 6.10

Experiment "**ORIGINAL**": carried out by using the original BFM-POM code without any implementation of deposition/resuspension process. The organic matter benthic-pelagic coupling is therefore defined by the deposition process only.

The resuspension process, described in section 4.4 was introduced in the following experiments.

Experiment "**BASE**": the deposition/resuspension process is introduced, but it is governed only by the current induced bottom stress.

Experiment "**BASEW**": the monthly time series of significant wave height and period described in section 5.2 were introduced and the bottom stress value is therefore affected also by the wave motion.

Finally a set of process oriented simulations were carried out by superposing to the monthly wave data time series an artificially increased wave motion. The characteristic of the increased wave motion are as follow:

- Duration: $\Delta t_w = 10days$
- Period of oscillations: $T = 4s$
- Height of the waves: $h_s = 1m$

5.5 Experiments definition

The timing of the increased wave motion period has been chosen on the basis of the phytoplankton dynamics as simulated in the "**ORIGINAL**" experiment depicted in Figure 6.10. The wave events have been imposed before, during and after every period of phytoplankton growth. In the figure are visible 3 different periods of active growth, here after called peaks: 2 surface peaks (one in late January and one in early December) and 1 peak close to the bottom (in September). The aim is to observe the effects of the resuspension on the Phytoplankton cycle. Above are described the results obtained by the different experiments described in the previous chapter.

Chapter 6

Results

All the numerical experiments were run for 5 years (1800 days) under repeating (perpetual year) monthly varying forcing. At the 5th year the model reached a stable repeating cycle. Therefore results shown focusing on the last integration year.

6.1 ORIGINAL case: no resuspension

The first experiment was carried out with the original model implementation: there is no resuspension and deposition is defined by a fixed deposition velocity. Therefore the bottom flux is due to Deposition only.

Figure 6.1 shows the annual cycle of the chlorophyll (a) and Particulate organic carbon (b) concentrations.

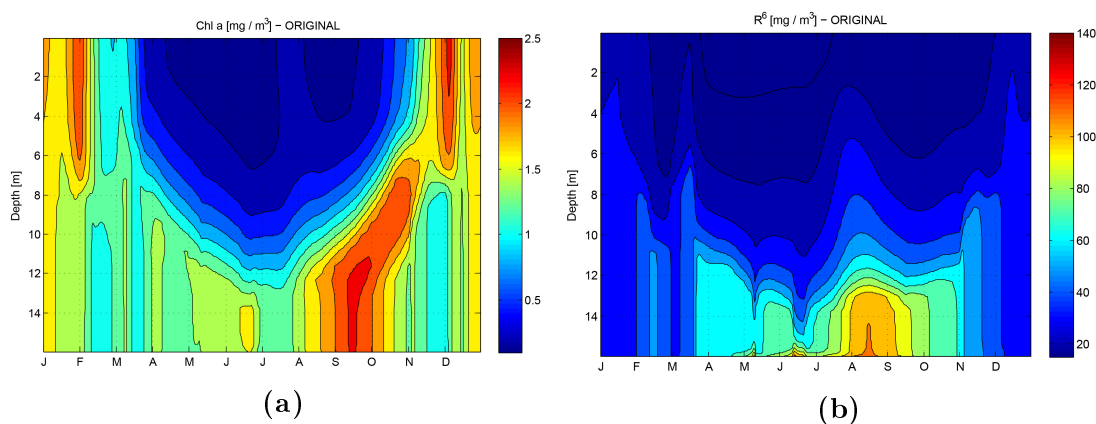


Figure 6.1: Annual evolution of the 5th year simulated of Chlorophyll-a and POC for the **ORIGINAL** experiment.

Phytoplankton (Figure 6.1a) shows two periods of surface blooming in the late

winter/early spring and in late autumn. Such cycle is well known for mid latitude ocean. In the northern Adriatic sea it depends mostly on the annual cycle of the vertical stratification structure that regulate the nutrient supply into the euphotic zone (Vichi et al. (2003)). For the summer period the simulation indicates also a significant Phytoplankton development in the lower water column depending on the increased light penetration and on the nutrient availability arising from organic matter recycling in the water column and in the sediment. In fact the particulate carbon cycle (Figure 6.1b) shows that organic matter accumulates near the bottom in the summer period and the corresponding increase of the benthic organic matter due to the deposition processes is showing in Figure 6.2a.

Finally is reported also the concentration of the filter feeders which presents different peaks in correspondence of the Detritus increase (Figure 6.2b).

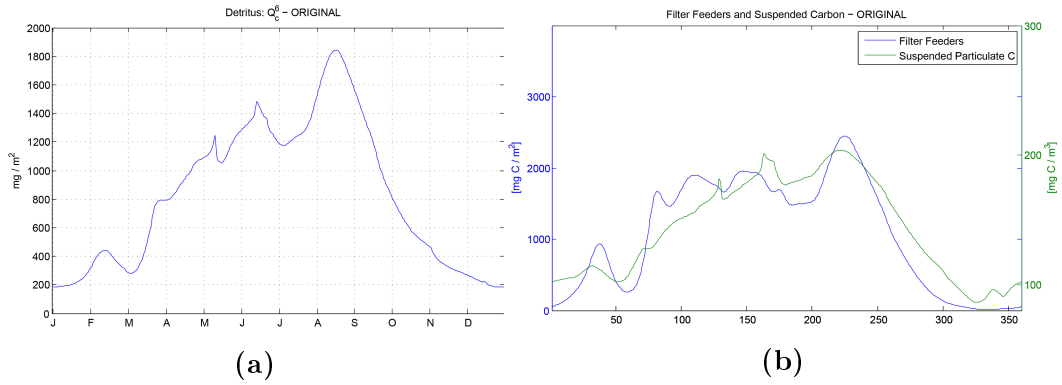


Figure 6.2: Annual time evolution of concentration of detritus (a) and filter feeders with the total carbon suspended (POC + Phytoplankton) (b) for the **ORIGINAL** case. The concentration of all the variables increases during the late-spring and summer.

6.2 BASE case: mean current resuspension

In this experiment the Deposition/Resuspension submodel is introduced using the climatological wind forcing described in the chapter 5. No wave forcing is applied.

The bottom stress is generated only by the mean circulation current and is shown in Figure 6.3. The figure shows that the critical stress value (τ_{crit}), above which resuspension occurs, is exceeded only for few days in January (the period of stronger winds).

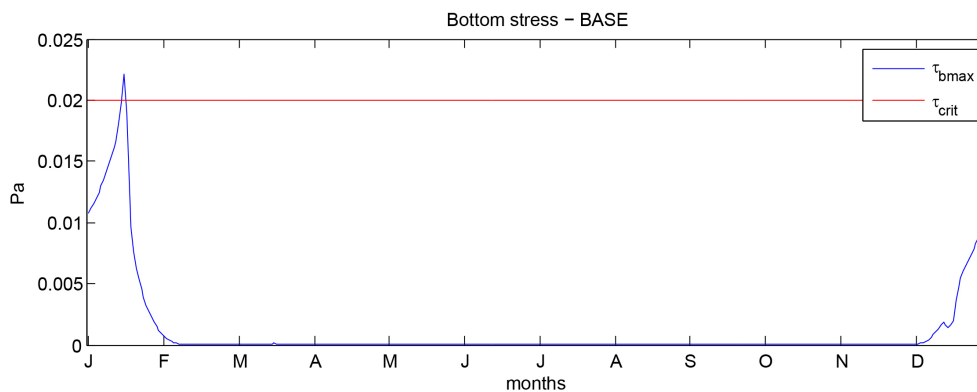


Figure 6.3: Bottom stress without wave motion on the surface (principally wind driven).

Activating the Deposition/Resuspension submodel with these setting determines the increase of the organic particulate in the water column in the period characterized by a bottom stress value exceeding the critical threshold (see Figure 6.5a). The Particulate is characterized by a strong upward propagation along the water column up to the surface. This happens because the process occurs in winter, that is to say, in a period during which the water column is well mixed (see Figure 6.4). This allows the propagation of the resuspended detritus through a significant portion of the water column.

The quantity of resuspended organic detritus is relatively high and, as soon as the bottom stress falls below the critical value the organic matter is quickly deposited back at the bottom. Is also visible an opposite effect after the resuspension when the POC reaches values slightly lower than those of the **ORIGINAL** case, more evident in figure in the last days of March. This trend is the opposite in the summer during which the increase of POC, already observed in the **ORIGINAL** case, is slightly enhanced.

Is possible to notice also a small change in the phytoplankton cycle due to resuspension. The behavior is parallel to that of the POC. In Figure 6.5b is visible a slightly decrease of chl-a close to the surface after the resuspension episode, as

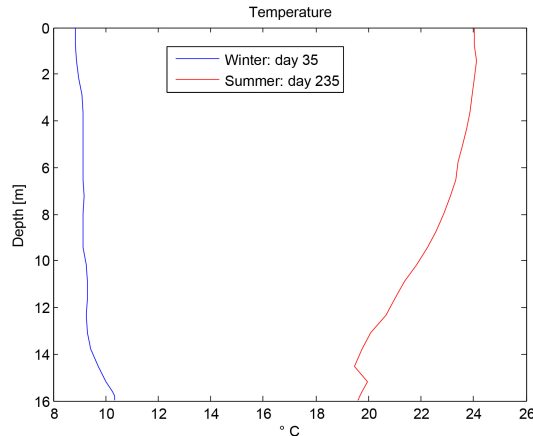


Figure 6.4: The Temperature vertical profiles verified during the two resuspension events: in February (blue), in August (red).

for the lower layers in the next months. This is maintained until the beginning of summer when, as described for POC, is recorded a weak phytoplankton increase (with respect to the **ORIGINAL** case) near the bottom. However, the phytoplankton cycle remains very similar to the one arising from the **ORIGINAL** experiment.

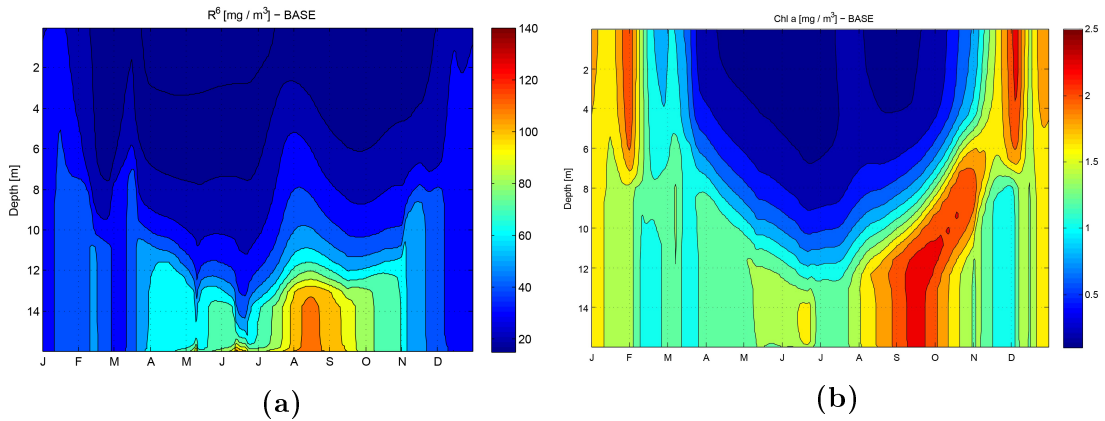


Figure 6.5: Annual time evolution of Chlorophyll-a and Carbon component of organic particulate (POC) concentration for the **BASE** experiment. Is evident the increasing of POC in all the column when $\tau_{bmax} > \tau_{crit}$ (January).

The resuspension of sediments is evident also by looking at the benthic organic Detritus shown in Figure 6.6a. The Resuspension is active in early/mid-January, period in which the benthic detritus reaches its minimum value. The figure shows also a strong increase after the resuspension event. Finally, in tuning with the other two variables, also Detritus shown an higher values during summer season. This benthic Detritus peak is matched by a corresponding increase of the filter

6.2 BASE case: mean current resuspension

feeders biomass due to the enhanced availability of suspended matter (Figure 6.6b).

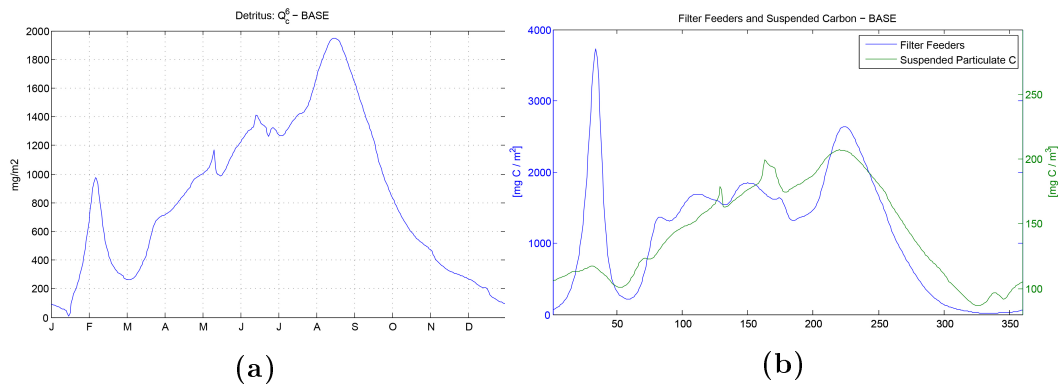


Figure 6.6: Annual time evolution of the concentration of detritus (a) and filter feeders with the total carbon suspended (POC + Phytoplankton) (b) for the **BASE** case. For detritus are evident 2 principal point of divergence with the **ORIGINAL** case: the decrease in early-January because of the resuspension; the strong increase after resuspension. For the filter feeders is recorded a strong increase in early February.

6.3 BaseW case: base-wave resuspension

In this experiments the waves are introduced and τ_w is computed.

The two bottom stresses, due to current and waves, are calculated using, respectively, the Equation 4.21 and 4.22.

By introducing the wave motion at the surface, τ_{bmax} shows several peaks through all the simulations (see Figure 6.7). The highest value is recorded in mid-November, when the wave period exceeds 4s and the height is $\approx 0.5m$ (see Figure 5.6 in chapter 5).

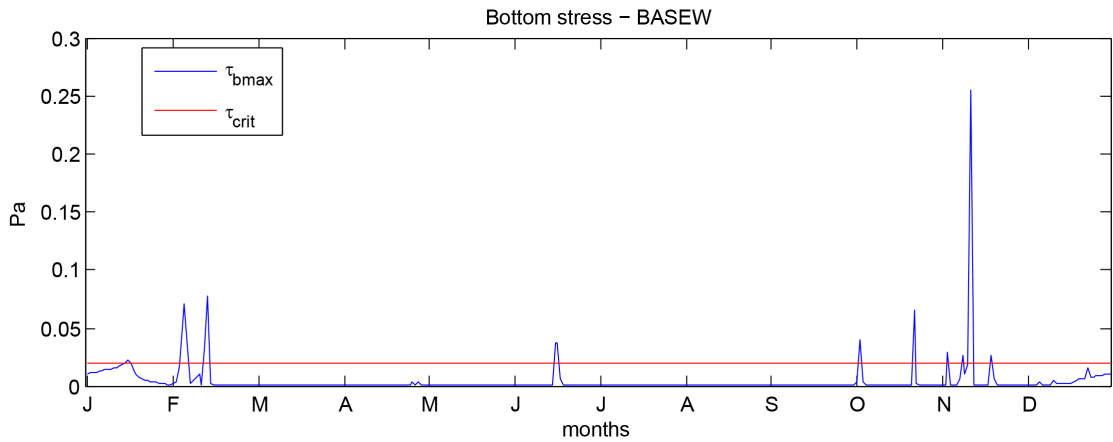


Figure 6.7: Maximum bottom stress introducing wave motion on the surface. The episodes of overcoming of the τ_{crit} are increased and occur at different moments of the year.

In this experiment, the resuspension generated is therefore greater than in the **BASE** case and also the deposition is reduced.

The immediate effect is an increase of POC in the water column in correspondence of the principal wave events. Three more important group of events occur in February, June and November (see Figure 6.8a).

The Phytoplankton follows the trend seen in the previous experiment (Figure 6.8b). Only a small difference is noted due to the resuspension event recorded in June, when the Phytoplankton shown a slight reduction. More visible is the increase of the water column POC. In the Figure 6.8a are evident the different Resuspension events through the increase of the Particulate especially in February, in June and different episodes in autumn. Because of the abundance of benthic detritus (see Figure 6.9a), the resuspended particulate flux in summer period is significant. The resuspension mechanism uplifts benthic organic matter, but, differently from the winter resuspension events, these cannot reach the surface and are blocked near the bottom (due to the increasing stratification) where interact with the other biogeochemical individuals.

6.3 BaseW case: base-wave resuspension

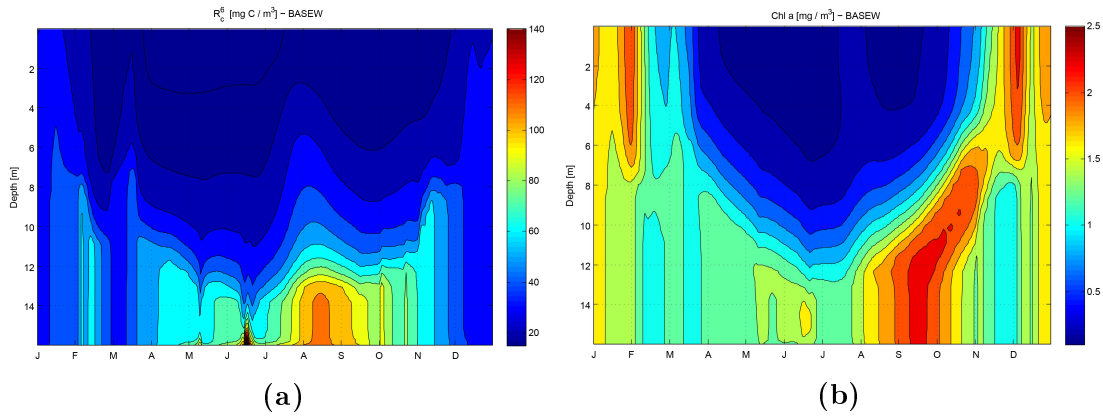


Figure 6.8: Annual time evolution of the concentration of Chlorophyll-a and Carbon component of organic particulate (POC) in the **BASEW** experiment. Are evident the increases of POC in correspondence of the more important waves events.

The resuspension on the benthic detritus can be noticed in Figure 6.9a. Interesting is the shape of the resuspension events already noticed for the January resuspension event in the previous experiment: after the initial decrease of Detritus is recorded an increase of it (see the mid-June event).

As seen also in the previous cases, the filter feeders change in the same way of the detritus (Figure 6.9b). The concentration shows a new high peak in mid-June.

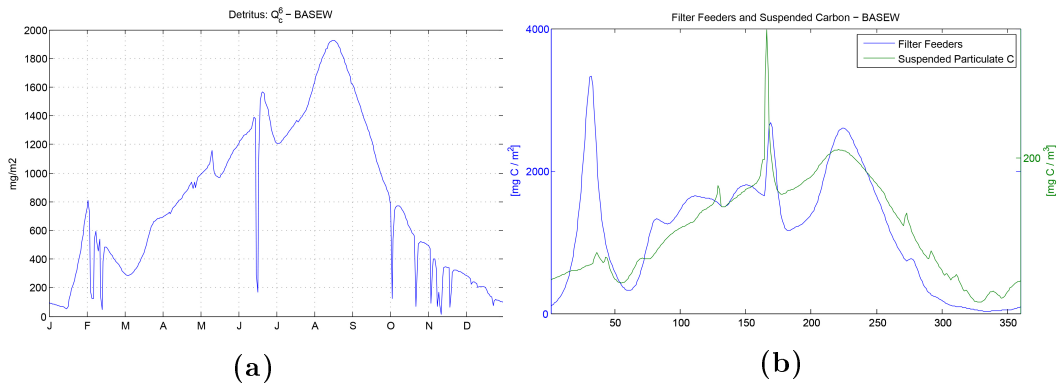


Figure 6.9: Annual time evolution of the concentration of detritus (a) and filter feeders with the total carbon suspended (POC + Phytoplankton) (b) for **BASEW** case. Are evident all the resuspension events, packable in three different groups: late-Winter, mid-June, Autumn.

Wave events

As specified in the previous section, 9 more experiments have been performed introducing ad-hoc waves events close to the 3 different period of phytoplankton growth described previously (Figure 6.10).

Wave events have been imposed periodically for all the 5 years of each numerical simulation according to the perpetual forcing structure adopted.

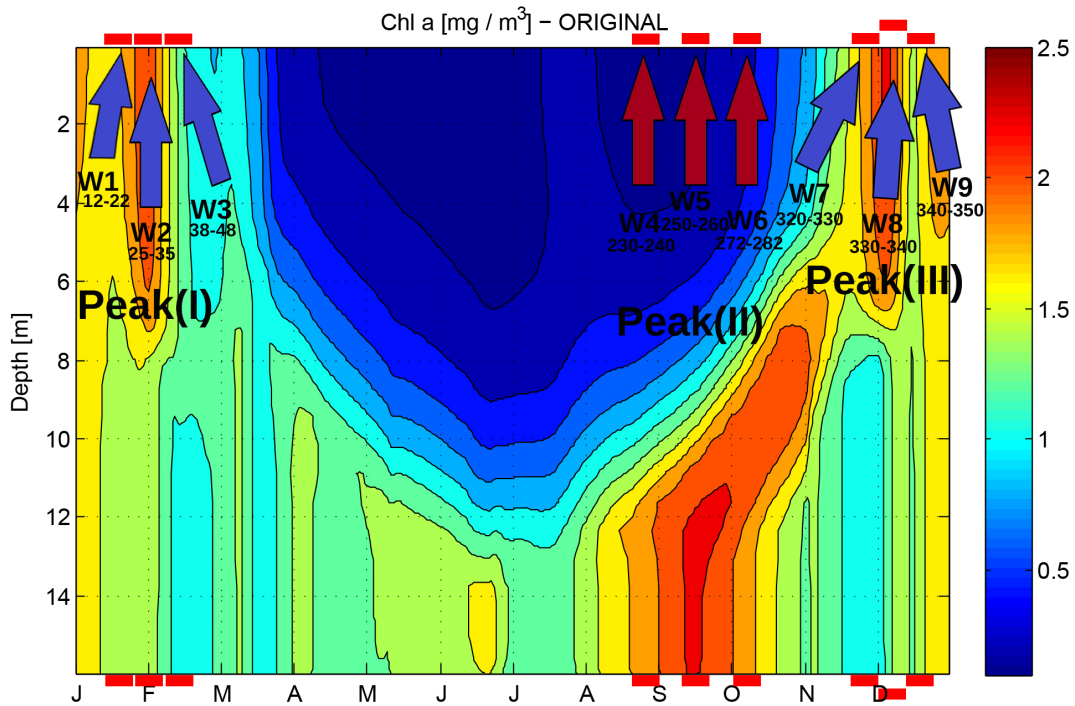


Figure 6.10: Timing of the waves events imposed during the experiments, located on the annual time evolution of the concentration of the chlorophyll-a in **ORIGINAL** case. The experiments are divided in 3 group referring to the 3 visible phytoplankton blooms called: peak(I), peak(II), peak(III). These blooms are 2 at the surface and 1 at the bottom. The arrows show the time location of the experiments.

6.4 Peak I: W1-W2-W3 cases

The first series of waves events is inserted before, during and after the Phytoplankton surface bloom in February (case **W1**, **W2** and **W3** respectively; see Table 5.1).

In Figure 6.11 is shown the temporal evolution of the POC vertical distribution for the **BASEW** case (top right), and the concentration differences between case **BASEW** and the **W1**, **W2**, **W3** cases. Same approach is used for the Phytoplankton concentration.

In Figure 6.11 is visible the different timing of the resuspension events for the three

6.4 Peak I: W1-W2-W3 cases

different cases. As noticed also in the previous case, the POC propagates upward arriving close to the surface in all the the cases. This is due also to the low winter stratification. The most evident resuspension event is the **W3** case, when the wave event is imposed after the development of the surface phytoplankton bloom. In all the three cases after the end of the event, the POC sink back to the bottom and all the three events do not determine any further variability in the POC dynamics.

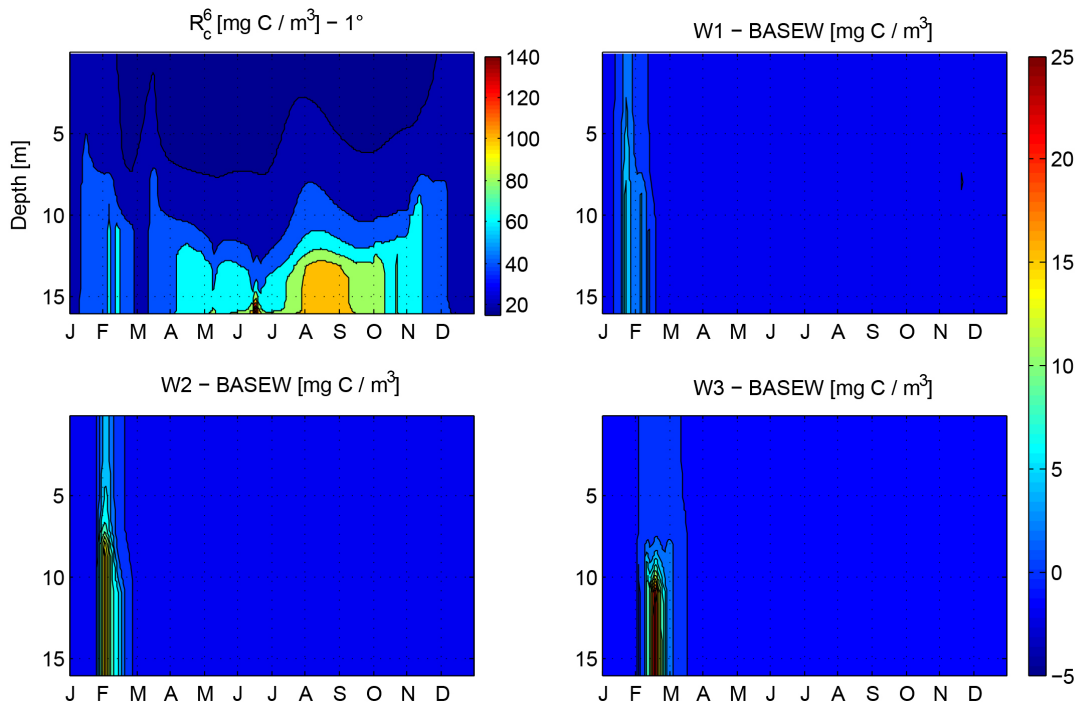


Figure 6.11: Annual time evolution of the concentration of POC for **BASEW** (top right) and the differences of concentration between case **W1** (top left), **W2** (bottom right) and **W3** (bottom left) and case **BASEW**.

Changes induced by the wave event on the phytoplankton concentration are quantitatively minimal (see Figure 6.12), but the timing of the event seems to impose some qualitative difference. In fact in the case **W1** and **W2** the immediate effect induced by the resuspension is a decrease of the phytoplankton concentration along almost the whole water column. However, after the end of the resuspension event the lower half of the water column experience a (however modest) increase of the phytoplankton biomass. This pattern is not repeated in the **W3** case, since the occurrence of the resuspension event, after the onset of the phytoplankton bloom, determines the absence of the biomass increase.

The behavior of the benthic detritus is parallel to the POC time evolution. Its concentration decrease during the resuspension events (different for all the last 3 cases) and remain slightly lower during the rest of the year (Figure 6.13).

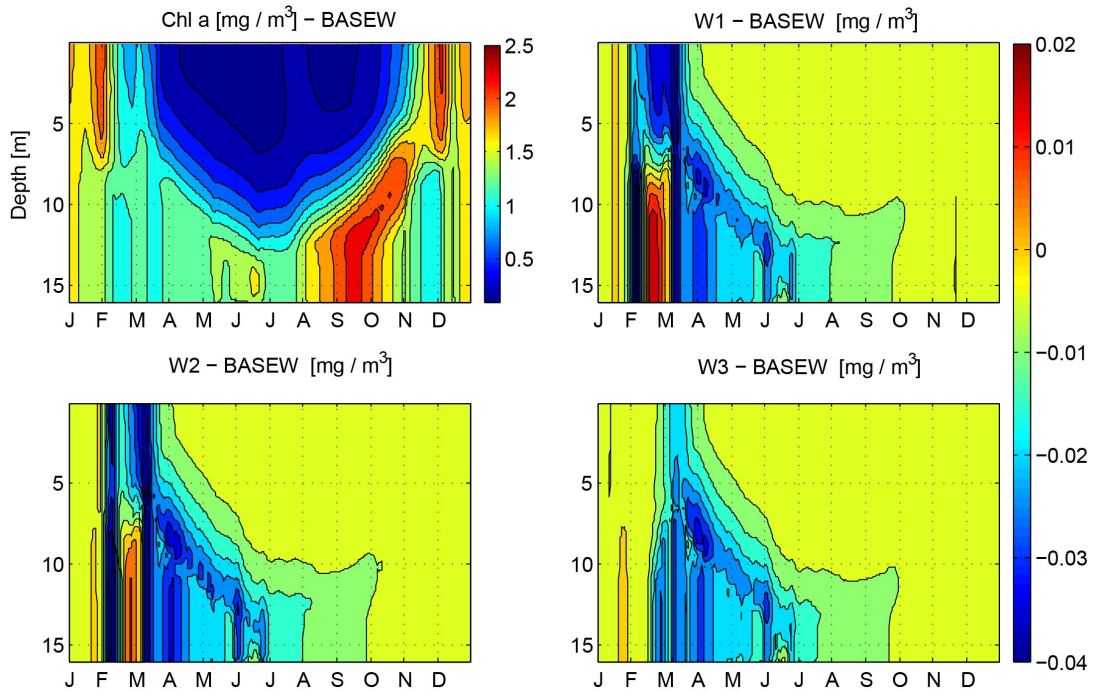


Figure 6.12: Annual time evolution of the concentration of chlorophyll-a (Phytoplankton) for **BASEW** (top right) and the differences of concentration between case **W1** (top left), **W2** (bottom right) and **W3** (bottom left) and case **BASEW**.

The Filter Feeders concentration in the 3 different cases increases close to the resuspension event in the early-February as visible in Figure 6.14. So the peak recorded in the **BASEW** cases is further increased and the growth of the Filter Feeders is encouraged.

6.4 Peak I: W1-W2-W3 cases

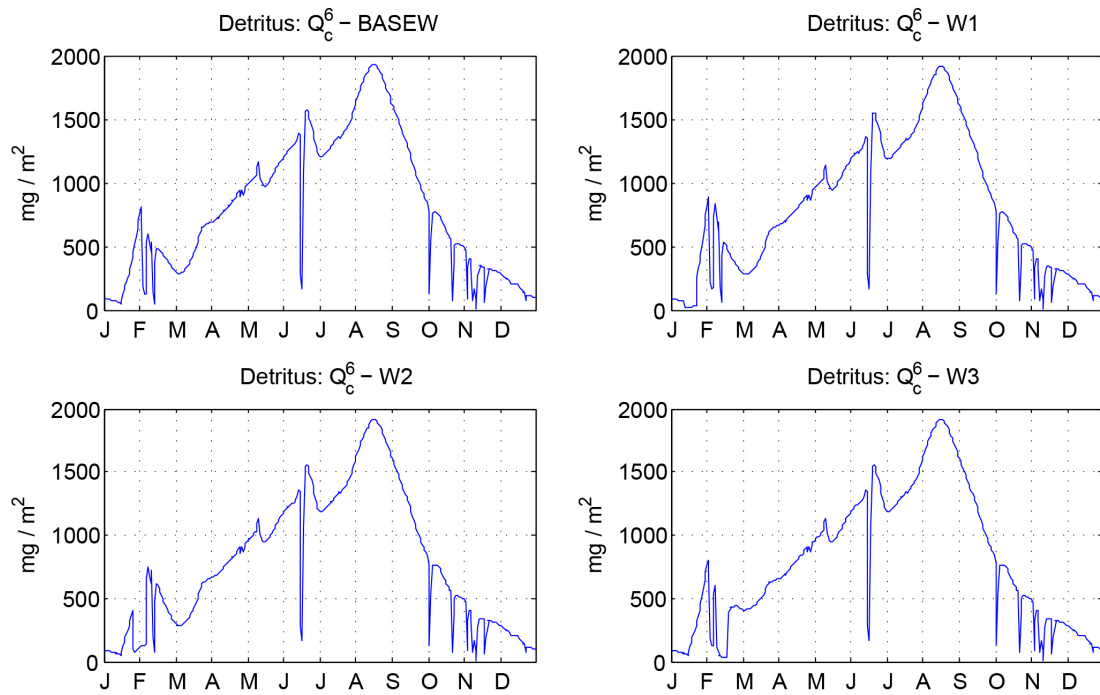


Figure 6.13: Annual time evolution of the concentration of detritus for **BASEW** (top right), **W1** (top left), **W2** (bottom right) and **W3** (bottom left) cases.

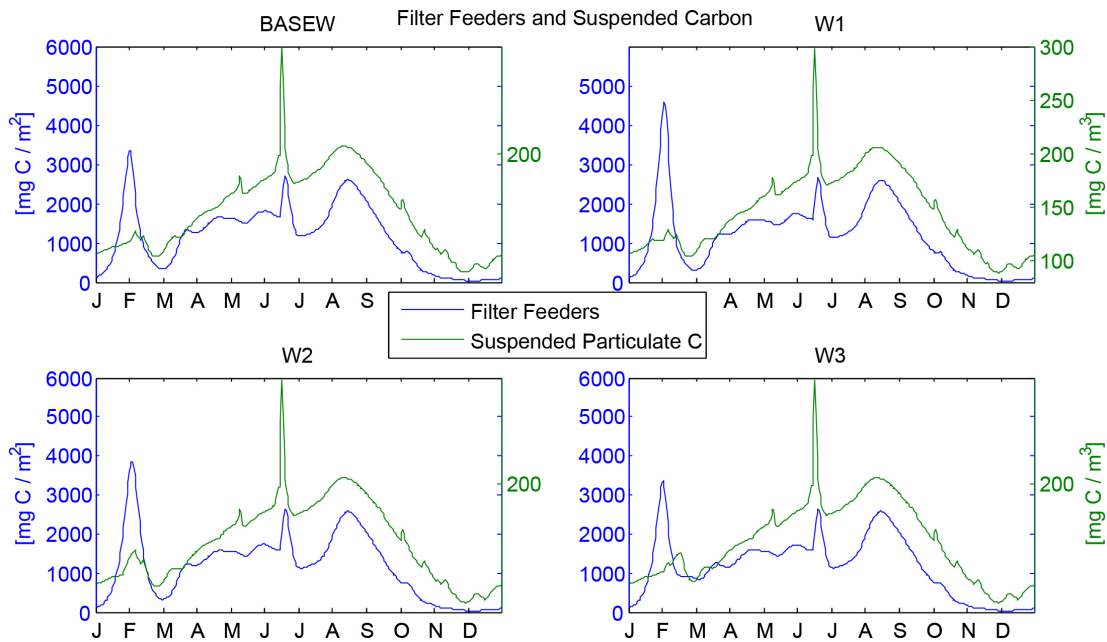


Figure 6.14: Annual time evolution of the concentration of filter feeders with the total carbon suspended (POC + Phytoplankton) concentration time distribution for **BASEW** (top right), **W1** (top left), **W2** (bottom right) and **W3** (bottom left) cases.

6.5 Peak II: W4-W5-W6 cases

The summer phytoplankton growth near the bottom is the strongest one of the **ORIGINAL** case (see Figure 6.10). In this period (as described in section 5.5) the phytoplankton biomass has a significant development starting from the bottom in late summer and extending to shallower depth in the following months.

The POC distribution in the water is shown in Figure 6.15. Compared to the previous cases the quantity of Carbon resuspended is larger, because of the higher concentration of the benthic detritus in this period of the year (see below). However, the carbon resuspended is only minimally extending to the upper water column due to the water column stratification.

Observing the time distribution of *chl-a* shown in Figure 6.16 it could be noticed that the resuspension events induce on the primary producers biomass the same pattern of temporal evolution previously described for the experiment **W1** and **W2**, that is to say an initial decrease followed by a subsequent biomass increase in the period immediately following the event. Such pattern is however limited to the lower half of the water column since (as previously stated) the density stratification limits the upward extension of the resuspended matter.

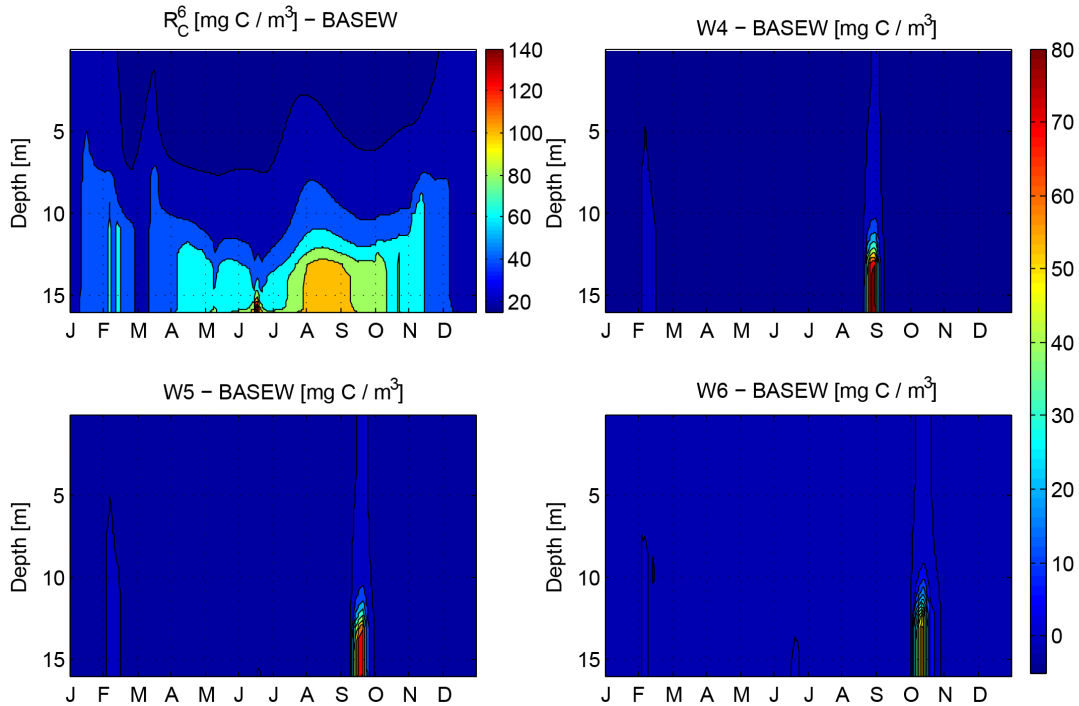


Figure 6.15: Annual time evolution of the concentration of POC for **BASEW** (top right) and the differences of concentration between case **W4** (top left), **W5** (bottom right) and **W6** (bottom left) and case **BASEW**.

6.5 Peak II: W4-W5-W6 cases

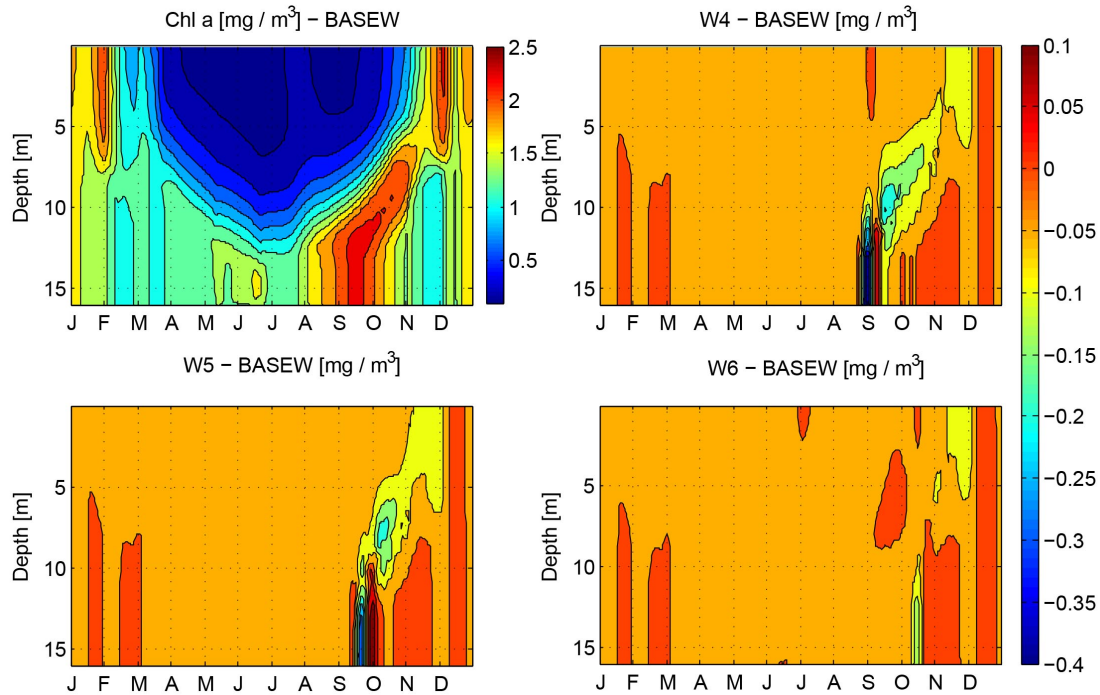


Figure 6.16: Annual time evolution of the concentration of chlorophyll-a for **BASEW** (top right) and the differences of concentration between case **W4** (top left), **W5** (bottom right) and **W6** (bottom left) and case **BASEW**.

The time series of the benthic detritus concentration show the resuspension events (see Figure 6.17) those remove quite all the Detritus. Like the previous cases also in this is evident the strong increase of the concentration after the resuspension.

As seen before, the concentration of the Filter Feeders follows the concentration of the Detritus. The higher peak is recorded in the case **W4**, because of the large concentration of Detritus in that case.

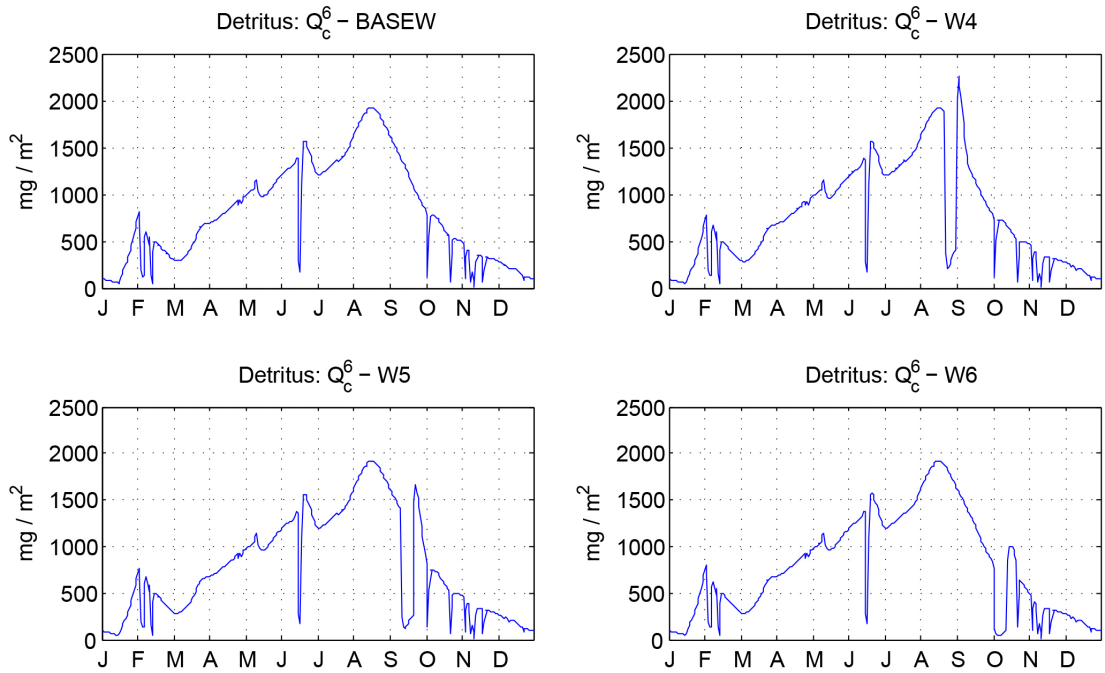


Figure 6.17: Annual time evolution of the concentration of detritus for the cases **BASEW** (top left), **W4** (top right), **W5** (bot left), **W6** (bot right) cases.

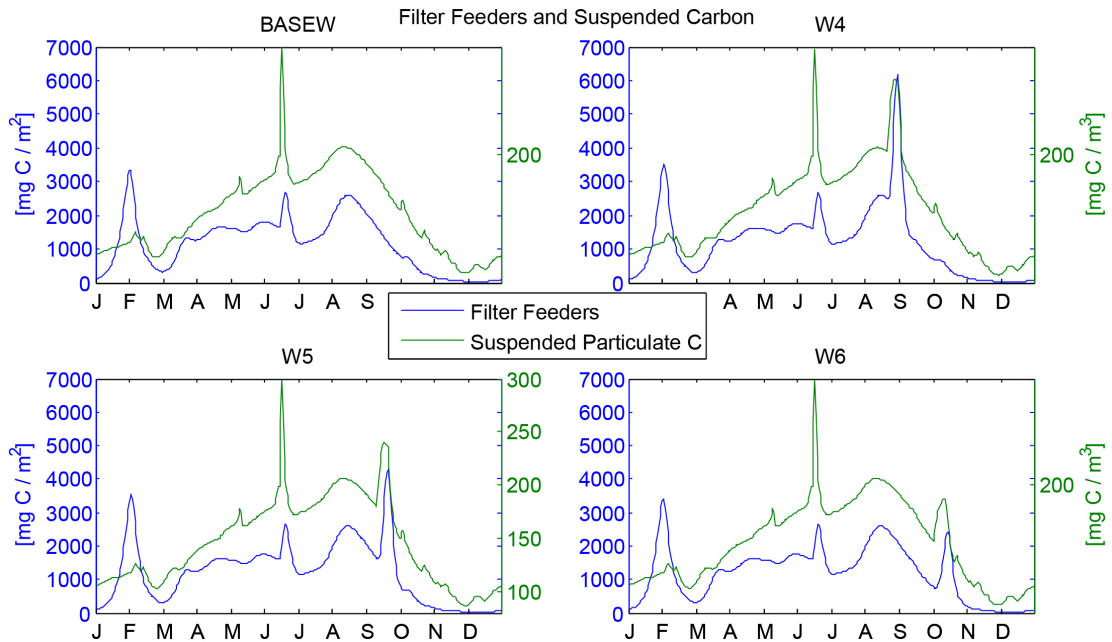


Figure 6.18: Annual time evolution of the concentration of filter feeders with the total carbon suspended (POC + Phytoplankton) concentration time distribution for the cases **BASEW** (top left), **W4** (top right), **W5** (bot left), **W6** (bot right) cases.

6.6 Peak III: W7-W8-W9 cases

The last group of experiments refer to the wave events imposed around the last surface bloom (**W7**, **W8**, **W9**) occurring in December (see Figure 6.10).

In order to describe the effects that wave events imposed under the three waves grouped under the peak(III), it has to be recalled that the wave events were periodically imposed along the full 5 years, length of the simulation. Therefore, given the vicinity of the wave events to the end of the simulation, in order to describe better the changes arising from the imposed wave events, will be shown the distribution of the biogeochemical processes across the last two simulation years.

Figure 6.19 shows the POC concentration for the **BASEW** and the differences with the different cases relative to the peak(III). The three resuspension events are visible. In all three cases, it can be noted the extension of the resuspension event. The increase of the POM concentration extends to the whole water column with a concentration vertical gradient defining a decreasing concentration toward the surface. In this respect the outcome of this simulation is not much different from the previous peak(I) experiment. However, the evolution of the POC cycle of vertical distribution has a quite different evolution in the relatively long period (about 2 months). In fact, differently from the peak(I) experiments, the POC concentration does not revert quickly to value comparable to those obtained in the **BASEW** experiment, but persist in time slowly decreasing for about 2 months and in experiments **W8** and **W9** undergo ever to a slight increase toward the end of February-beginning of March. After the POC concentrations undergo to a sharp decrease all along the water column.

The different evolution of the POC vertical distribution cycle is matched also by the corresponding phytoplankton evolution (see Figure 6.20). Overall the wave event imposes a local and immediate phytoplankton decrease all along the water column, followed by a local increase in the lower part of the water column. However, experiment **W7** and **W8** differentiate by the experiment **W9**, in that the phytoplankton increase near the bottom is more extended in time, subsequently concentrations have a value evidently lower with respect to the **BASEW** case and the recovery to the background concentration is slower. In this respect experiment **W9** resembles closely the three peak(I) experiments.

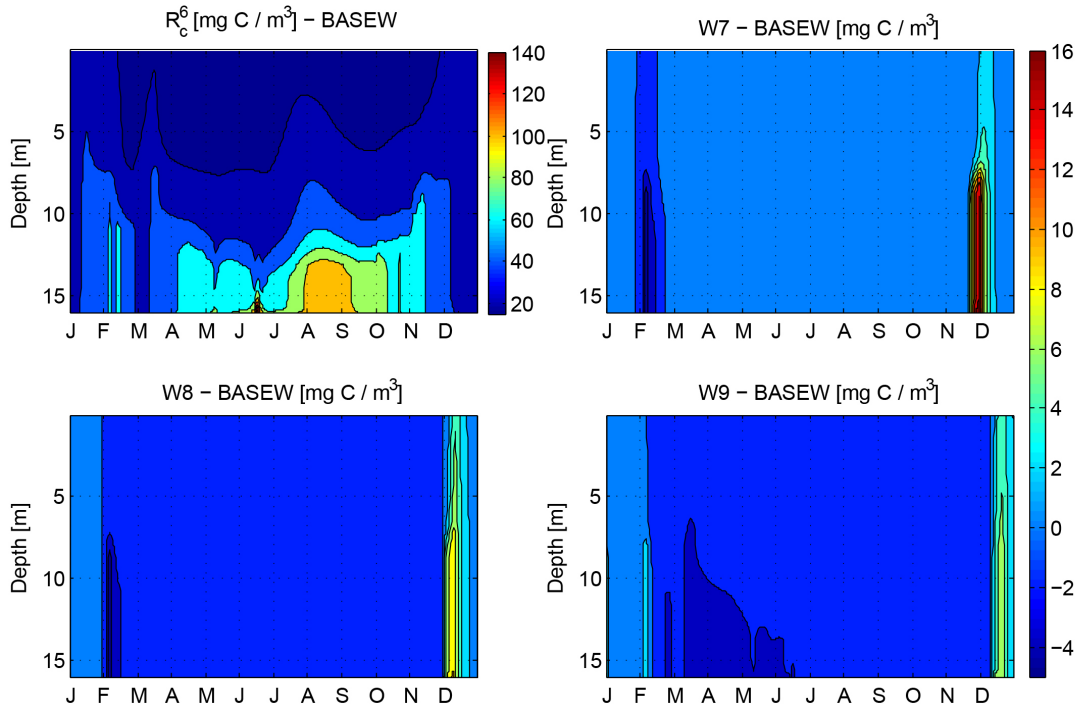


Figure 6.19: Annual time evolution of the concentration of POC for **BASEW** (top right) and the differences of concentration between case **W7** (top left), **W8** (bottom right) and **W9** (bottom left) and case **BASEW**.

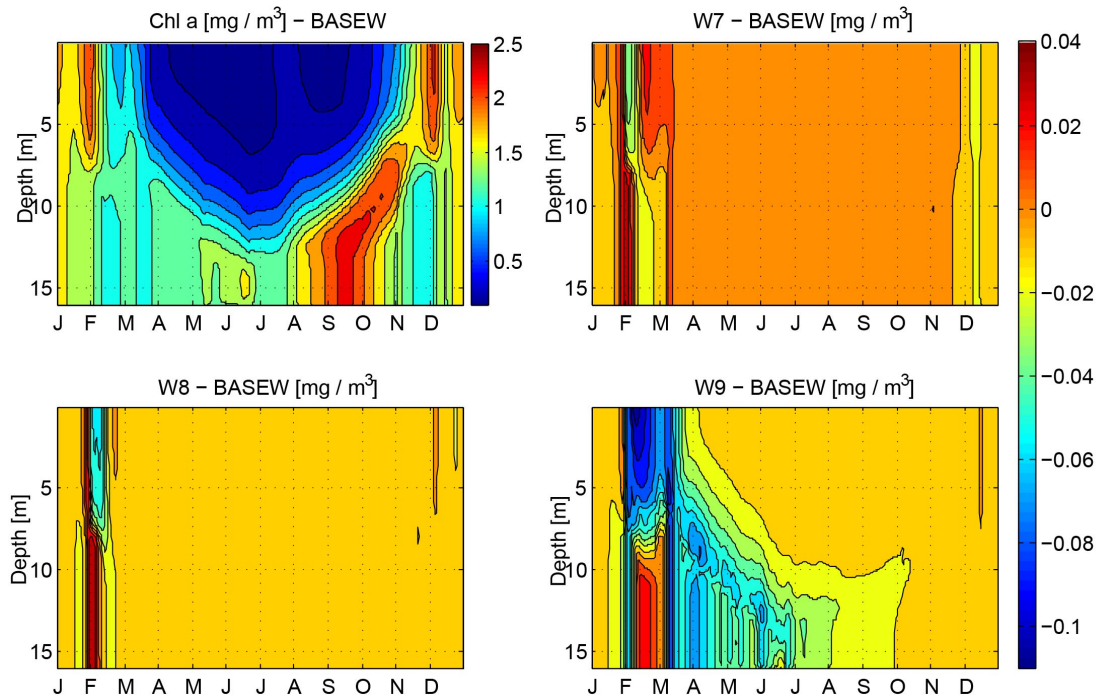


Figure 6.20: Annual time evolution of the concentration of chlorophyll-a for **BASEW** (top right) and the differences of concentration between case **W7** (top left), **W8** (bottom right) and **W9** (bottom left) and case **BASEW**.

Looking at the benthic detritus annual cycle for the three experiments (Figure 6.21) is visible that the timing of the three different events is characterized

6.6 Peak III: W7-W8-W9 cases

by different concentration of that detritus: grater in case **W7** and lowest in case **W9**. This explains the different quantity of POM released in the water column in the three cases (see Figure 6.19). As for POC and phytoplankton, also the benthic detritus records in experiments **W7** and **W8** different concentration values in proximity of the resuspension event of early-February compared to the **W9**. Comparing the relative maximum of the concentration in that period in the first two experiments with that one in the case **BASEW** is visible a deformation: in **W7** and **W8** the increase starts earlier, but reaches lower values. Differently in experiments **W9** the concentration of benthic detritus reaches greater values than in the **BASEW** case.

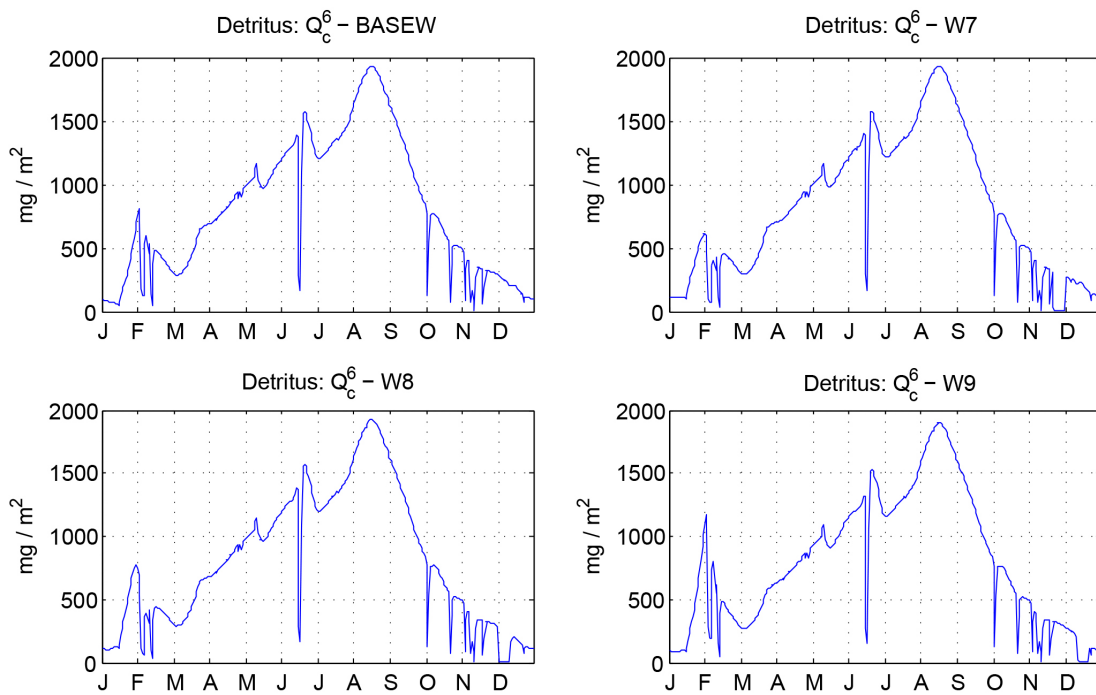


Figure 6.21: Annual time evolution of the concentration of benthic detritus for the cases **BASEW** (top left), **W7** (top right), **W8** (bot left), **W9** (bot right) cases.

The Concentration of the filter feeders (FF) respect the behavior already observed in the previous cases. The only explicit difference between the experiments is the reaction of the filter feeders in February, to the event of resuspension, as shown in Figure 6.22. In the figure is notable that this peak of FF has different reactions to the three different experiments: it decreases in **W7**, lightly decreases in **W8** and increases in **W9**, as seen for the benthic detritus concentration.

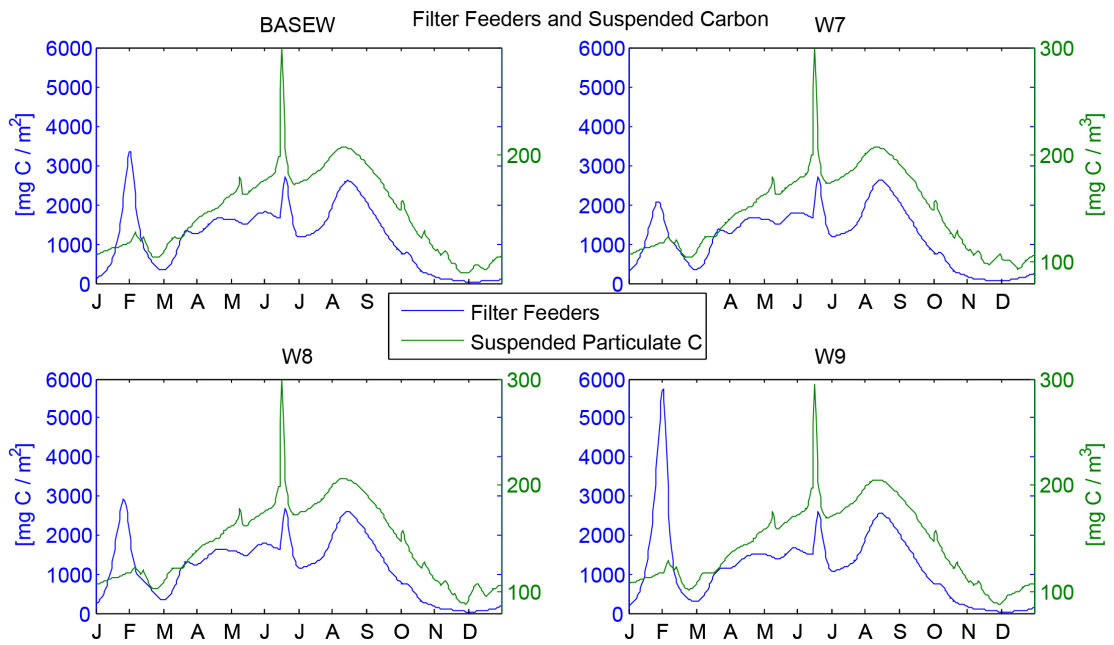


Figure 6.22: Annual time evolution of the concentration of filter feeders with the total carbon suspended (POC + Phytoplankton) concentration time distribution for the cases **BASEW** (top left), **W7** (top right), **W8** (bot left), **W9** (bot right) cases.

Chapter 7

Discussion

The results shown in the previous chapter indicate some point of interest regarding the coupled physical-biogeochemical system dynamics and are analyzed and discussed in the following. In particular the focus is on:

- bottom stress values and formulation
- stratification effects
- phytoplankton/bacteria interaction and extinction coefficient time evolution

7.1 Maximum bottom stress calculation

Hereafter are done some considerations about the definition of the maximum bottom stress τ_{bmax} .

As explained in the section 4.4 the applicability of the parametrization of the combined bottom stress formulated by Wang and Pinardi (2002) and Grant and Madsen (1979) is not verified because the two velocities u_c (mean current) and u_w (wave orbital velocity) are not comparable. The consequence is that the stress τ_{bmax}^{gm} calculated using this method (defined by eq.4.23) doesn't represent correctly the maximum bottom stress.

The empirical parametrization of the stress proposed by Soulsby (1995) has been used in substitution. To show the difference between the 2 formulation, experiment **BASEW** has been run twice utilizing the Grant and Madsen (1979) and Soulsby (1995) parametrization. The corresponding yearly cycle of the maximum bottom stress, computed in the two cases, is shown in Figure 7.1.

It can be easily noted that the Grant and Madsen (1979) formulation of τ_{bmax} provides values clearly lower than those arising from the Soulsby (1995)

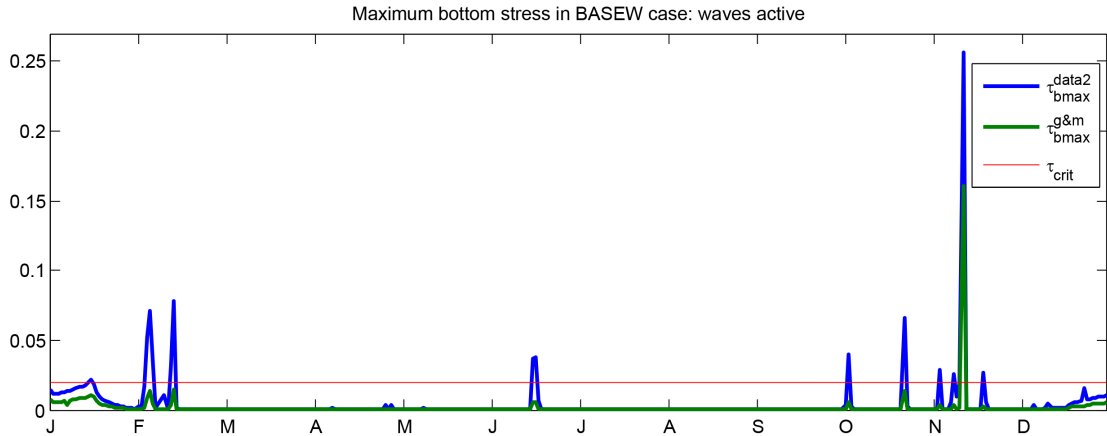


Figure 7.1: Annual cycle of the bottom maximum stress computed with the DATA2 method (dot blue) and with the Wang and Pinardi (2002) (green) in the experiment **BASEW**.

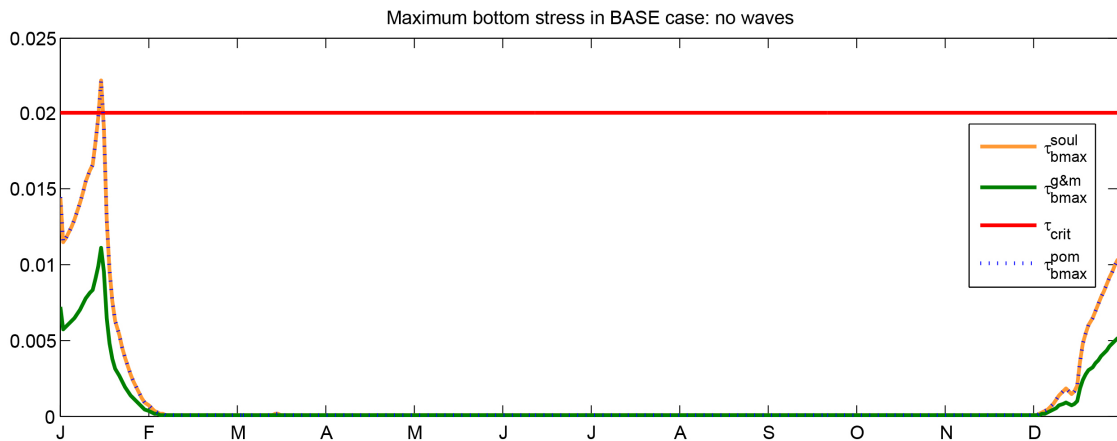


Figure 7.2: Annual cycle of the bottom maximum stress computed with the DATA2 method (dot blue) and with the Wang and Pinardi (2002) (green) in the experiment **BASE**, without wave motion.

formulation.

As a term of reference in Figure 7.2 it is reported also the cycle of the bottom stress computed in the **BASE** experiment using the two methods. It is recalled that in this experiment waves are not applied and therefore the bottom stress is entirely depending on the current velocity. The figure reports also the bottom stress cycle computed the POM standard computation (see Equation 4.4).

The figure demonstrates that the Grant and Madsen (1979) formulation used in absence of waves is unable to replicate the bottom stress computed in a standard way, while the Soulsby (1995) method exactly replicates it. This result justified the adoption of the Soulsby method.

7.2 Resuspension and mixing conditions

The experiments carried out indicate quite clearly that the distribution of the resuspension POM along the water column depend on the magnitude of the bottom stress, but also on the timing of the resuspension event with respect to the stratification mixing conditions of the water column.

For instance, the POM resuspended in the winter season (see experiments peak(I) and peak(III)) experience a much greater redistribution along the water column than with respect to the peak(II) cases.

The importance of the stratification can be understood by looking at the yearly cycle of the turbulent diffusive coefficient K_m (Figure 7.3a) in coordination with the corresponding cycle of the particulate organic matter obtained in the **ORIGINAL** experiment (Figure 7.3b).

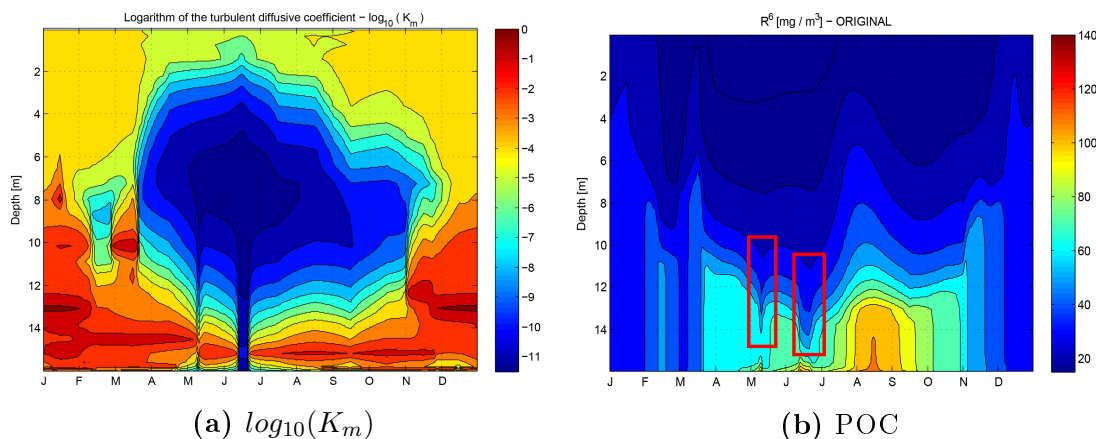


Figure 7.3: Time evolution of the logarithm of the turbulent diffusive coefficient K_m (a) and of POC (b) in **ORIGINAL** case. In POC figure are pointed out the two moments when K_m strongly decreases.

The figures show how the diffusivity varies near the bottom: it's maximum in the winter season and lower in the Summer with two minimum in early-March and mid-June. This two minimum in K_m determine the decrease of the POC concentration in the bottom layers.

This consideration implies the importance of the timing of the resuspension events during the year, as already stressed in the previous chapter. Looking at the winter events (experiments peaks (I) and (III)) can be noted how the events that are imposed closer to the end/start of the year generates a perturbation of the system which persists longer (Figures 6.12 and 6.20). This happens even if the concentration of the benthic detritus in the winter period is at the lowest (Figure 6.2a). It is interesting to observe the time evolution of the differences between

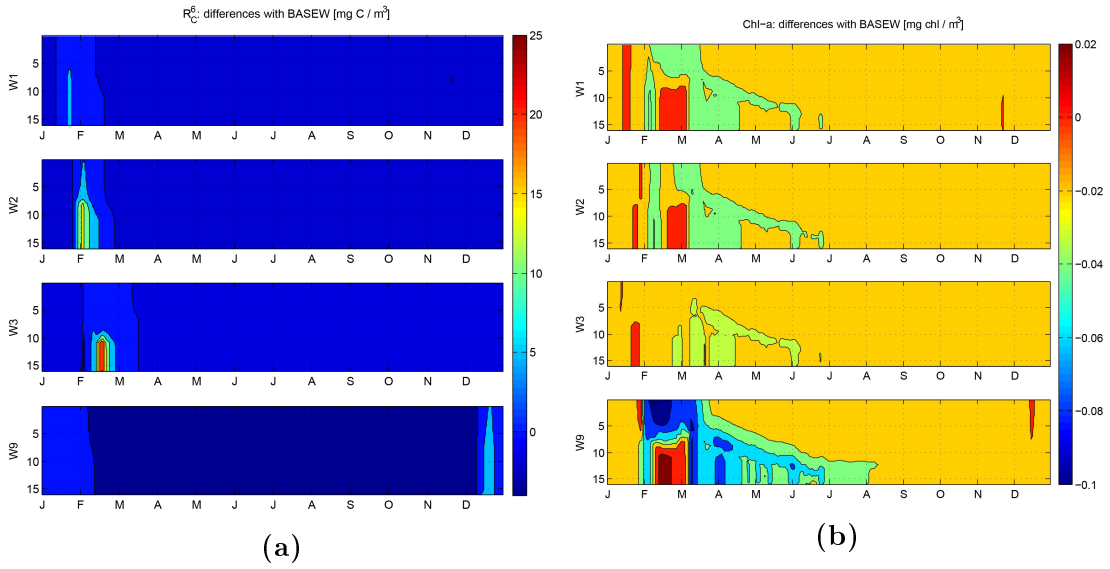


Figure 7.4: Time evolution of the concentration of the POC (a) and the phytoplankton (b) for the cases relative to the peak(I) and the case **W9**.

the phytoplankton concentration of the experiments **W1** and **W9** (Figure 7.4b), with respect to experiment **BASEW** (Figure 6.8a): the two time evolutions look like very similar and show a perturbation which persists until July. The cases **W2** and **W3** are characterized by a larger (with respect to **W1**) detritus resuspension, but the perturbation of the phytoplankton cycle is slightly lower.

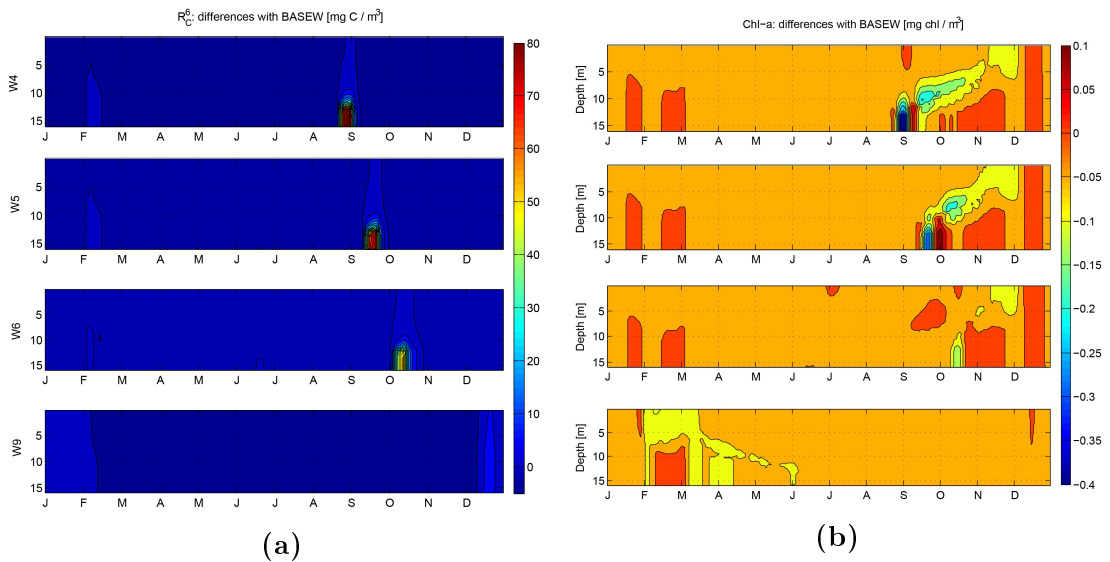


Figure 7.5: Time evolution of the concentration of the POC (a) and the phytoplankton (b) for the cases relative to the peak(III) and the case **W9**.

The same happens in the cases relative to the peak(II) (see Figure 6.16) as the quantity of resuspended POC is more larger (Figure 7.5a), but the dynamic

7.2 Resuspension and mixing conditions

conditions are less turbulent. The consequence is that the resuspension strongly influence the biogeochemical system only in the short term, as is visible in the phytoplankton concentration (Figure 7.5b), and not in the long term, because the POM settles again quickly to the seabed.

Thus it can be concluded that the timing of the resuspension events is very important and significantly influence the vertical distribution of the water column properties. In particular, when the POM is resuspended in winter season it can remain in the water column for several months influencing the other biogeochemical variables as phytoplankton and bacteria. Otherwise the summer events are characterize by a greater quantity of detritus resuspended which influence the biogeochemical system in the short term, but not in the long term, because of the strong stratification.

7.3 Phytoplankton/bacteria relationship during the resuspension event

Hereafter is analyzed the behavior of the biogeochemical variables in the cases relative to the peak(II), with particular reference to the phytoplankton and bacteria temporal evolution in the experiment **W4**.

As a general rule the onset of the resuspension event determines the almost immediate decrease of the phytoplankton biomass (Figure 7.6a). The phytoplankton decrease is matched by a corresponding increase of the bacteria biomass (Figure 7.6b). After the end of the resuspension event the opposite behavior has been observed (phytoplankton increase and bacteria decrease).

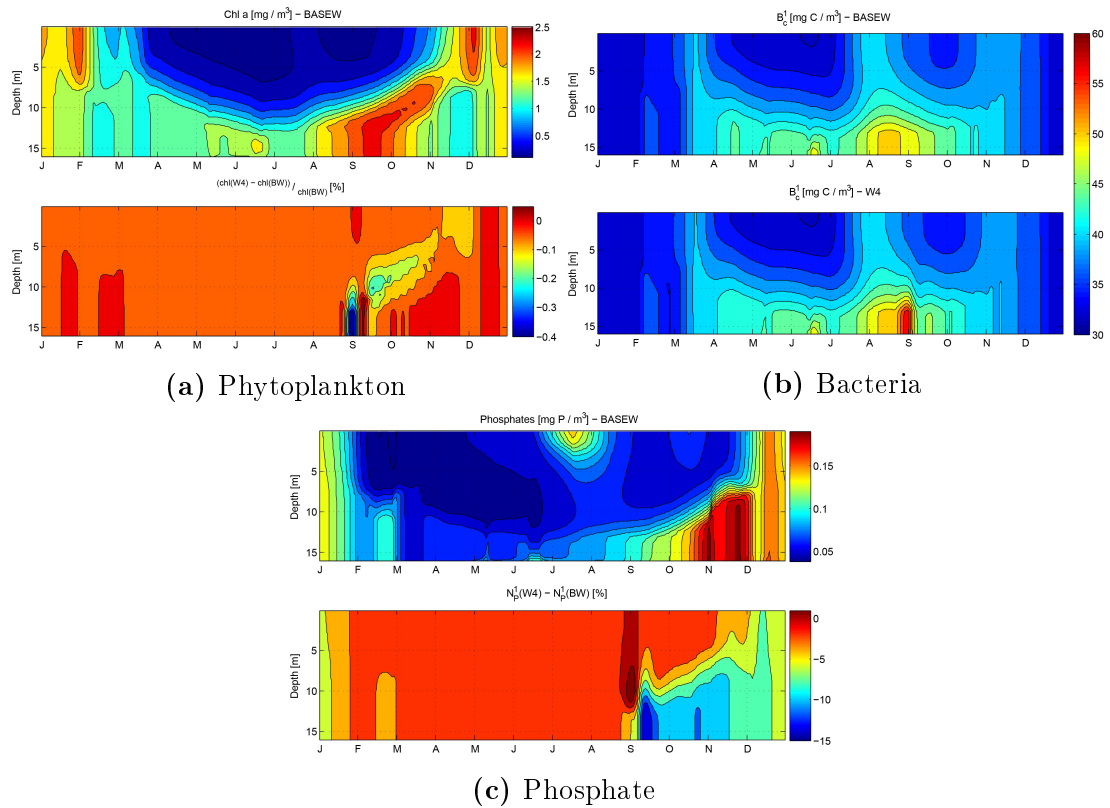


Figure 7.6: Annual time distribution of the profiles of phytoplankton (a), Bacteria (b) Phosphate nutrients (c) for the cases **BASEW** (top) and **W4** (down). For the phytoplankton and phosphate are reported the relative percentile differences (bottom). It is visible the strong decreasing of the phytoplankton and the sudden increase of the bacteria during the resuspension event. The N_1P concentration decrease later, after the resuspension event.

This pattern in the temporal evolution of the two biogeochemical state variables can be explained by investigating the modification of the qualitative and quantitative properties of the resuspended organic matter determined by the resuspension event. In fact the onset of the resuspension determines an increase

7.3 Phytoplankton/bacteria relationship during the resuspension event

of the carbon available to bacteria. The resuspension determines also a change in the carbon to phosphorus and the carbon to nitrogen ratio that approach the "Redfield Ratio", but still remain below the optimal value:

$$C : P \equiv 106 : 1 \quad [\text{Redfield et al. (1963)}]$$

The annual cycle of the C/P ratio in the particulate organic matter is shown in Figure 7.7a. The increased availability of carbon embedded into organic matter, having a non optimal carbon to nutrient ratio, causes the bacterial internal ratio to remain "unbalanced" below the optimal ratio for bacteria (Goldman et al. (1987)) as shown in Figure 7.7b.

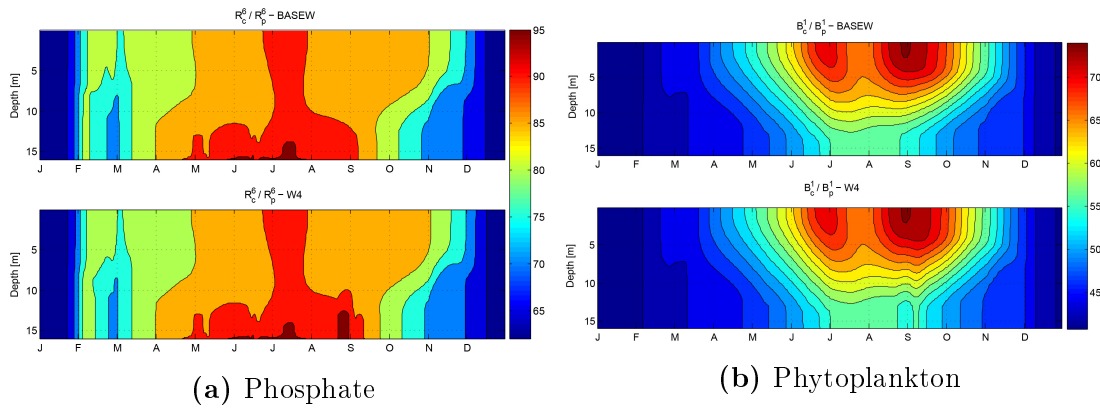


Figure 7.7: Annual time distribution of the profiles of C/P in the POM (a) and in the bacteria (b) for the cases **BASEW** (top) and **W4** (down).

The unbalanced carbon to phosphorus ratio in the organic matter and the increased carbon availability force the bacteria to turn to the phosphate as a source of phosphorus, therefore competing with the phytoplankton for the nutrients utilization (Figure 7.6c), as described in Baretta J.G. and Hansen A.S. (1998). A schematic of the phosphorus flow in absence and with resuspension is given in Figure 7.8a and 7.8b respectively, where the thickness of the arrows drawn is proportional to the magnitude of the different fluxes.

In the **ORIGINAL** experiment is verified this cycle (see the sign of the flux between benthic sediment and POM).

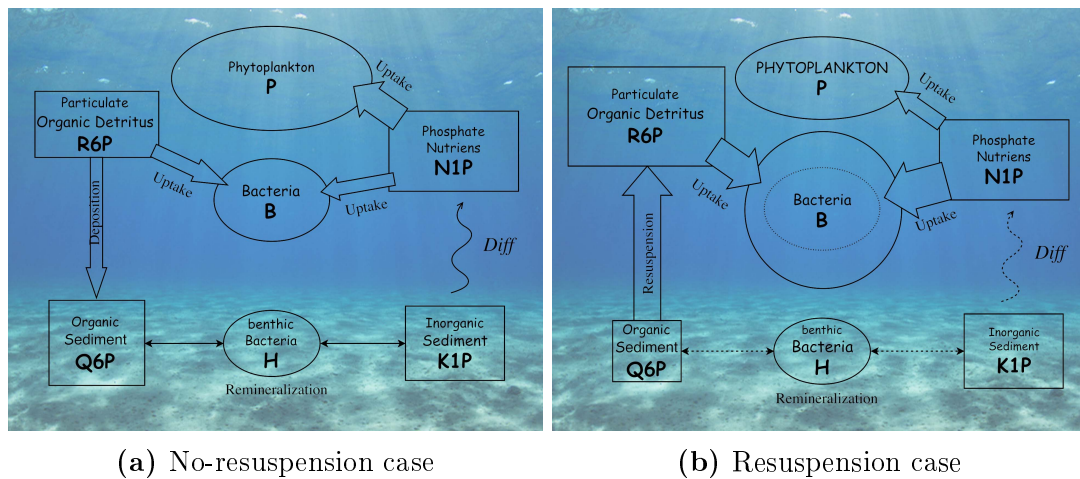


Figure 7.8: Normal benthic-pelagic cycle of phosphate for the no-resuspension case (a) and during the resuspension (b).

Light extinction

The decrease of the phytoplankton during the resuspension event is also enhanced by the increased turbidity of the water column as shown by the temporal evolution of the light extinction coefficient (Figure 7.9).

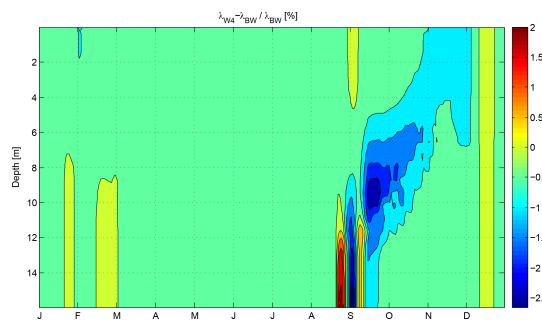


Figure 7.9: Relative difference between the total extinction coefficients in the cases **W4** and **BASEW**.

The increase of the phytoplankton concentration immediately after the end of the resuspension event is due to the occurrence of the condition that previously led to the enhanced bacteria activity. In fact immediately after the end of resuspension event the particulate organic matter quickly sinks back into the benthic realm and this leads to a reduction of the suspended organic matter available to bacteria.

Chapter 8

Conclusions

A better definition of the bottom stress could be improved with the utilization of a more physical formulation, however the results obtained with the Soulsby's parametrization are widely satisfactory.

The numerical experiments carried out have highlighted in preliminary way the impact that the purely physical sedimentary organic matter resuspension event might have on the coupled pelagic-bacteria system in a shallow coastal domain. The work involved the implementation of the resuspension procedure to the organic matter lying in the bottom sediments.

The implementation evolved from a previous work applied to the inorganic suspended sediment and involved an improvement in the definition of the computation of the bottom stress determined by wave action on the bottom.

In absence of wave motion, the particular features of the NAS basin, generate in the winter months the resuspension of organic detritus, which are then transported to the upper layers by the intense mixing typical of this period of the year. This POM becomes available to the transport processes operated by the mean circulation of the basin. Although the low concentration of the detritus in winter reduce the impact of the phenomena and a low quantity of POM is injected into the water column. The low concentration and the removal by advective motion prevent from a significant reaction of the pelagic biology. However, the POM resuspended in winter months remains more time in the water column, because of the low stratification, and can generate perturbation on the other biogeochemical variables also several months after.

More significant is the reaction of the biogeochemical system when the resus-

pension events occur in the summer period when the seabed is rich in organic matter. The resuspension of the detritus provokes the decrease of the concentration of phytoplankton due to the enhanced bacteria activity, that, given the increased carbon availability, operate a stronger uptake of inorganic nutrients that are subtracted to the phytoplankton.

This formulation of the deposition/resuspension flux gives satisfying results, but in at the application of the strong wave stresses the decrease of Detritus looks like very fast. Thus a deeper study has to be done in the parametrization of the resuspension velocity which regulates the resuspension flux. Actually the value used is $w_{res} = 10^{-7}m/s$ in order to reach a maximum flux of the magnitude of $10^{-4}mg/m^{-2}s$, as predicted by Ariathurai and Krone (1976).

Ringraziamenti

Sono molto grato di aver frequentato questo corso di studi, di aver potuto inseguire quelli che sono i miei desideri e aver imparato a studiare il nostro pianeta da diversi punti di vista che affascinano e rilanciano alla ricerca continua sempre aperta alla novità, alla scoperte spesso non scontate.

In questo lungo tragitto tanti sono stati gli stimoli e i compagni di viaggio, che come per il viaggio di Tobia si sono rivelati veri angeli, portatori di una novità che si rivela piano piano e ci rende nuovamente fanciulli pieni di vita. Condividendo questo cammino ho scoperto che la ricerca della Vita piena non è mai scontata e ti presenta traguardi e gioie non immaginati. L'aprirsi alla bellezza e alla gioia che ogni condizione rivela cambia e rinnova lo sguardo che può liberarsi dalle fatiche e le schiavitù delle paure e dell'immobilismo, spirituale, sociale e psicologico. Questo ho imparato, che cambiare questo mondo è possibile, renderlo più bello, più ospitale per tutti è possibile, ma richiede Verità e comprometersi (cosa per me assai ardua).

E quindi grazie a tutti i compagni "d'armi" qui in università. In primis al prof. Marco Zavatarelli che ha avuto l'onere particolarmente difficile di accompagnarmi alla fine di questo lavoro condividendo conoscenze e idee, ma anche fatiche e fragilità quotidiane. Un grosso grazie a Gelsomina che invece ha dovuto solo sopportarmi e correggermi anche nelle banalità giorno dopo giorno. Grazie ai miei nuovi compagni di corso: Alessio ilMaestroAlfonso Andrea Arianna Eleonora Enrica Francesco Giulio Jacopo Matteo Matteo Sara Tommaso; e a quelli vecchi, soprattutto Cecilia Giovanni Michele Veronica, siete stati un'aiuto prezioso!

In particolare voglio ringraziare i miei genitori e la mia famiglia che mi hanno sostenuto senza remore in questo traguardo, con anche troppa gentilezza, senza farmi mai mancare il sostegno e il confronto. In particolare grazie Chiara e Jack per aver condiviso le diverse "battaglie" quotidiane e grazie a Laura e Fra per essere un esempio e un sostegno anche la bellezza delle vostre famiglie. Grazie a voi cugini/fratelli Luca e Matteo.

Un piccolo grande ringraziamento (tra le righe, tranquilla) all'Elli ... solo Dio

sa quanti punti sta guadagnando in questo cammino insieme. Grazie perché mi richiami ogni giorno alla Vita non facendomi mai mancare la tua vicinanza e simpatia. Se ho fatto dei passi in questi anni lo devo soprattutto alla tua presenza.

Grazie ai miei amici nella fede, ai fratelli maggiori, ai minori. Grazie a Beppe, p.PierPaolo, d.Paolo per il grande sostegno che mi hanno donato in questi anni; grazie a tutti gli amici che mi hanno accompagnato pazientemente e con l'esempio (siete troppi, ci vorrebbe un'altra tesi): in parrocchia, al MISMO, in campo, nel quartiere a tutti voi GRAZIE!

Tutti questi grazie per un nuovo traguardo, che è davvero INIZIO, si racchiudono in un grande grazie a Dio che continua a scommettere sulla mia vita con un'entusiasmo a dir poco sconvolgente, senza sconfitta.

Buon cammino a tutti noi, verso una vita sempre piú pienamente Umana !!

Bibliography

- Ariathurai, R. and Krone, R. B. (1976). Mathematical modeling of sediment transport in estuaries. *Estuarine Processes*, II:98–106.
- Asselin, R. (1972). Frequency Filter for Time Integrations.
- Baretta J.G., B. L. and Hansen A.S., R. B. (1998). An improved model of carbon and nutrient dynamics in the microbial food web in marine enclosures. 14:91–108.
- Blumberg, A. and Mellor, G. (1987). A Description of a Three-Dimensional Coastal Ocean Circulation Model.
- Butenschön, M. (2007). *Numerical simulations of the coastal marine ecosystem dynamics: integration techniques and data assimilation in a complex physical-biogeochemical model*. PhD thesis.
- Butenschön, M., Zavatarelli, M., and Vichi, M. (2012). Sensitivity of a marine coupled physical biogeochemical model to time resolution, integration scheme and time splitting method. *Ocean Modelling*, 52–53:36–53.
- Chao, S. (1998). Hyperpycnal and buoyant plumes from a sediment-laden river. *Journal of Geophysical Research*, 103(C2):3067.
- Clarke, S. and Elliot, A. J. (1998). Modelling suspended sediment concentrations in the Firth of Forth. *Estuarine, Coastal and Shelf Science*, 47:235–250.
- Clementi, E. (2013). Coupled wave-ocean modelling system in the Mediterranean Sea.
- Cosoli, S., Licer, M., Vodopivec, M., and Malacic, V. (2013). Surface circulation in the Gulf of Trieste (northern Adriatic Sea) from radar, model, and ADCP comparisons. *Journal of Geophysical Research: Oceans*, 118(11):6183–6200.

- Goldman, J. C., Caron, D. A., and Dennett, M. R. (1987). Regulation of gross growth efficiency and ammonium regeneration in bacteria by substrate c : N ratio. 32(6).
- Grant, W. D. and Madsen, O. S. (1979). Combined wave and current interaction with a rough bottom. *Journal of Geophysical Research: Oceans*, 84(C4):1797–1808.
- Lou, J., David J. Schwab, D. B., and Hawley, N. (2000). A model of sediment resuspension and transport dynamics in southern lake michigan. *Journal of Geophysical Research*, 105(C3):6591– 6610.
- Malacic, V. and Petelin, B. (2009). Climatic circulation in the gulf of trieste (northern Adriatic). *Journal of Geophysical Research: Oceans*, 114(7):1–15.
- McDonnell, A. M. P. and Buesseler, K. O. (2010). Variability in the average sinking velocity of marine particles. *Limnology and Oceanography*, 55(5):2085–2096.
- Mellor, G. L. and Yamada, T. (1982). Development of a turbulence closure model for geophysical fluid problems. *Reviews of Geophysics*, 20(4):851–875.
- Mussap, G., Zavatarelli, M., and Pinardi, N. (2015). A management oriented 1-D ecosystem model : implementation in the Gulf of Trieste (Adriatic Sea). *Journal of Geophysical Research - Oceans*, page 39.
- Mussap, G., Zavatarelli, M., Pinardi, N., and Celio, M. (2016). A management oriented 1–D ecosystem model: Implementation in the Gulf of Trieste (Adriatic Sea). *Regional Studies in Marine Science*, 6:109–123.
- Redfield, A., Ketchum, B., and Richards, F. (1963). The influence of organisms on the composition of sea-water.
- Signell, R. P., Chiggiato, J., Horstmann, J., Doyle, J. D., Pullen, J., and Askari, F. (2010). High-resolution mapping of bora winds in the northern adriatic sea using synthetic aperture radar. *Journal of Geophysical Research: Oceans*, 115(C4). C04020.
- Soulsby, R. (1995). Bed shear–stresses due to combined waves and currents. In M.J.F Stive, H.J. de Vriend, J. Fredsoe, L. Hamm, R.L. Soulsby, C. Teisson, J. W., editor, *Advanced in Coastal Morphodynamics*, chapter 4, pages 20–23. Delft, delft hydr edition.

BIBLIOGRAPHY

- Southard, J. (2006). Special topics: An introduction to fluid motions, sediment transport, and current-generated sedimentary structures threshold of movement.
- Vichi, M., Lovato, T., Lazzari, P., Cossarini, G., Gutierrez Mlot, E., Mattia, G., Masina, S., McKiver, W. J., Pinardi, N., Solidoro, C., Tedesco, L., and Zavatarelli, M. (2015). *The Biogeochemical Flux Model (BFM): Equation Description and User Manual. BFM version 5.1*. BFM Consortium.
- Vichi, M., Masina, S., and Patara, L. (2006). The Biogeochemical Flux Model (BFM). Technical report.
- Vichi, M., Oddo, P., Zavatarelli, M., Coluccelli, A., Coppini, G., Celio, M., Umani, S., and Pinardi, N. (2003). Calibration and validation of a one-dimensional complex marine biogeochemical flux model in different areas of the northern adriatic shelf. *Annales Geophysicae*, 21(1):413–436.
- Vichi, M., Pinardi, N., and Masina, S. (2007). A generalized model of pelagic biogeochemistry for the global ocean ecosystem. part i: Theory. *Journal of Marine Systems*, 64(1–4):89–109. Contributions from Advances in Marine Ecosystem Modelling Research, 27-29 June, 2005, Plymouth.
- Wang, H. and Pinardi, N. (2002). Modeling the dynamics of sediment transport and resuspension in the northern Adriatic Sea. *Journal of Geophysical Research*, 107(12):18–1–18–23.
- Wang, X., Pinardi, N., and Malacic, V. (2007). Sediment transport and resuspension due to combined motion of wave and current in the northern Adriatic Sea during a Bora event in January 2001 : A numerical modelling study. *Continental Shelf Research*, 27:613–633.